

Durham Research Online

Deposited in DRO:

06 August 2014

Version of attached file:

Published Version

Peer-review status of attached file:

Peer-reviewed

Citation for published item:

Bailiff, I.K. and French, C.A. and Scarre, C.J. (2014) 'Application of luminescence dating and geomorphological analysis to the study of landscape evolution, settlement and climate change on the Channel Island of Herm.', *Journal of archaeological science.*, 41 . pp. 890-903.

Further information on publisher's website:

<http://dx.doi.org/10.1016/j.jas.2013.10.014>

Publisher's copyright statement:

© 2014 The Authors. Published by Elsevier Ltd. This is an open access article under the CC BY license (<http://creativecommons.org/licenses/by/3.0/>).

Additional information:

Use policy

The full-text may be used and/or reproduced, and given to third parties in any format or medium, without prior permission or charge, for personal research or study, educational, or not-for-profit purposes provided that:

- a full bibliographic reference is made to the original source
- a [link](#) is made to the metadata record in DRO
- the full-text is not changed in any way

The full-text must not be sold in any format or medium without the formal permission of the copyright holders.

Please consult the [full DRO policy](#) for further details.



Application of luminescence dating and geomorphological analysis to the study of landscape evolution, settlement and climate change on the Channel Island of Herm

I.K. Bailiff^{a,*}, C.A. French^b, C.J. Scarre^a

^a Department of Archaeology, Durham University, South Road, Durham DH1 3LE, UK

^b Division of Archaeology and Anthropology, University of Cambridge, Downing Street, Cambridge CB2 3DZ, UK

ARTICLE INFO

Article history:

Received 11 April 2013

Received in revised form

29 September 2013

Accepted 13 October 2013

Keywords:

Luminescence dating

Geomorphological analysis

Island archaeology

Climate change

ABSTRACT

The optically stimulated luminescence (OSL) dating of sands and palaeosol horizons, sampled as part of an archaeological investigation and supported by geomorphological analysis, has been applied to identify critical stages in the development of the landscape on Herm, one of the Channel Islands that lies off the coast of Guernsey, on which megalithic monuments were constructed during the Neolithic period. In particular, there were three phases of significant aeolian activity during the prehistoric period, the onsets dated by OSL in this study to ca 4, 3 and 2.3 ka ago, where the first phase marked a significant change in the long term trend of aggradation of soils that persisted during the next two millennia. OSL ages were also obtained for palaeosols in which there was evidence of ploughing, placing this activity in the late 2nd millennium BC and the 4th and 13th centuries AD. The OSL ages for basal deposits of dune sands that cover the northern part of the island indicate that they were formed by phases of intense aeolian activity during the medieval period, commencing in the 13th century AD and continuing for several hundred years, which can be correlated with documented high intensity storms in the North Atlantic within the period 13th–15th centuries AD. The phases of significant aeolian activity dated by OSL to ca 4 and 2 ka ago can be linked with those detected in different regions of the North Atlantic coastal areas. The availability of chronologies for aeolian horizons provides a valuable tool in the study of the evolution of coastal landscape and how past coastal communities responded to climate change.

© 2014 The Authors. Published by Elsevier Ltd. This is an open access article under the CC BY license (<http://creativecommons.org/licenses/by/3.0/>).

1. Introduction

Amongst the islands that lie within the outer reaches of the British Isles, including Shetland, Orkney and the Western Islands to the north, the Isles of Scilly to the south, and the Channel Islands that lie in the Normanno-Breton Gulf (Fig. 1), there are relatively high concentrations of megalithic monuments that were constructed during the Neolithic period. On Herm the small chambered tombs, which have been studied since the 19th century (Kendrick, 1928), are distinctively aligned along a ridge between two hills located in the northern part of the island (Fig. 2). Several of these tombs and the associated prehistoric land surface are almost completely concealed by a thick layer of dune sand which has preserved a Neolithic landscape with activity marked by the construction of monuments, traces of settlement and cultivation. In a recently completed study (Scarre and French, 2013), a programme

of excavation, soil sampling, micromorphological analysis and dating was conducted to reconstruct the environmental history of northern Herm during the Holocene and to interpret the nature and extent of Neolithic activity on the island. As part of this work, optically stimulated luminescence (OSL) was applied to date the formation of the dunes, the burial of the prehistoric land surface and key stages in the development of the landscape. Aeolian sands and palaeosols were sampled to address several basic research questions, primarily focused on determining a) the age of the prehistoric land surfaces, b) when they were buried by sand dunes and c) the ages of key horizons in the development of the prehistoric palaeosol sequence. However, the OSL ages produced for key phases of aeolian activity on Herm also provide further data related to the issues of storminess in the N Atlantic region and, given its relevance to human settlement in coastal regions, we also discuss the Herm results in the context of the wider regional studies of climate change.

The application of OSL to dune chronology has become a topic of relevance to the study of climate change in coastal regions of NW Europe since the processes of aeolian transport and dune formation

* Corresponding author.

E-mail address: Ian.Bailiff@dur.ac.uk (I.K. Bailiff).

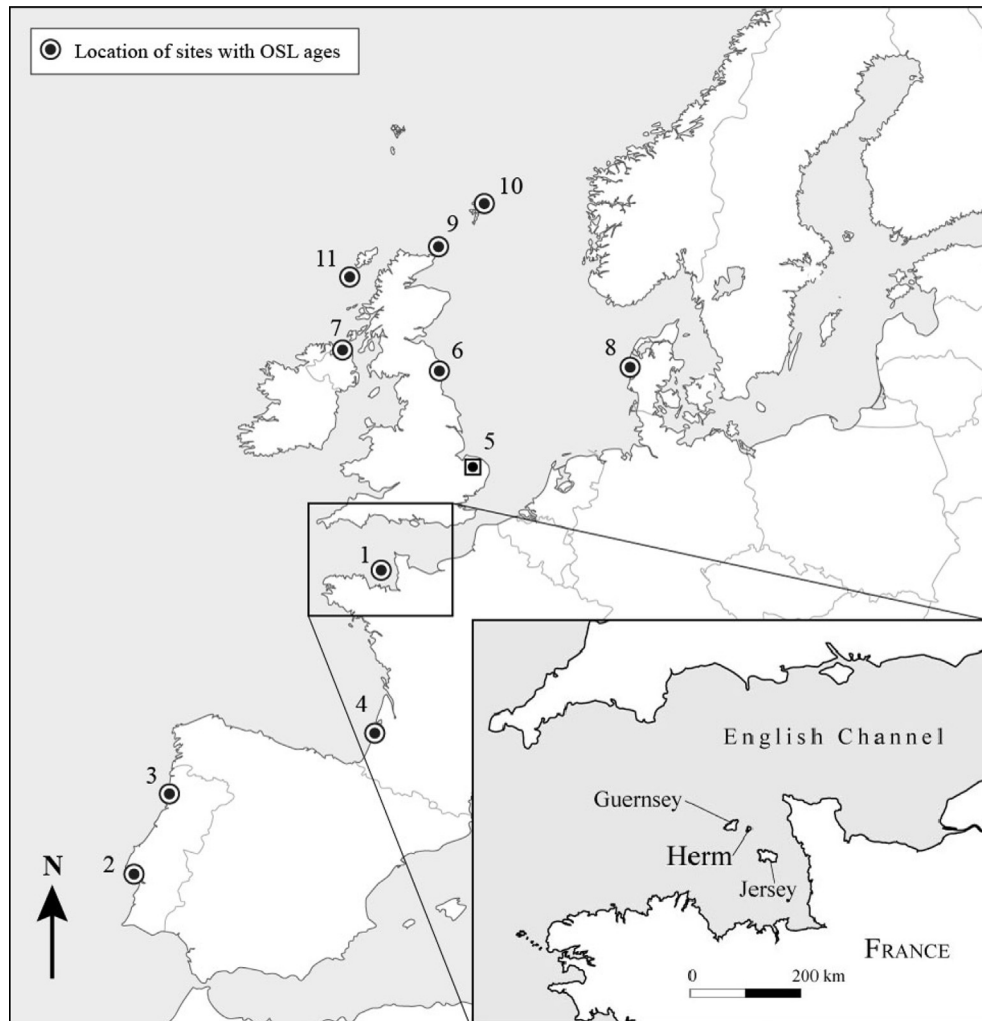


Fig. 1. Geographical map showing location of Herm and, with the exception of the inland site 5, other coastal sites in the North Atlantic region discussed in the main text, where OSL dating studies on dune sands have been reported: 1. Herm; 2. Portugal (Costas et al., 2012b); 3. Portugal (Clarke and Rendell, 2006); 4. Aquitaine (Clarke et al., 2002); 5. East Anglia (Bateman and Godby, 2004); 6. Northumberland (Wilson et al., 2001); 7. N Ireland (Wilson et al., 2004); 8. Jutland (Clemmensen et al., 2009); 9. Orkney (Sommerville et al., 2003, 2007); 10. Shetland (Sommerville et al., 2003); 11. Outer Hebrides (Gilbertson et al., 1999).

have been linked to storm events within the North Atlantic region (Lamb, 1977; Lamb and Frydendahl, 1991). In previous work on coastal archaeological sites in the Western Isles, Orkney, Shetland and on the NE English coast (Gilbertson et al., 1999; Sommerville et al., 2001, 2003, 2007), OSL ages identified periods of significant aeolian sand mobilization. In the most recently published study by Sommerville et al. (2007), two major phases of aeolian activity dated by OSL to ca 2000 BC and ca 1000 BC were associated with abandonment of the prehistoric settlement of Tofts Ness on Sanday, Orkney, and linked to enhanced North Atlantic storminess during the onset of periods of climate deterioration in N. Scotland. To explore the potential for using sand mobilisation and dune formation as a proxy record of climate change, various studies have applied OSL to date sand mobilisation in coastal regions (e.g., Wintle et al., 1998; Clarke et al., 1999; Orford et al., 2000; Clemmensen et al., 2001; Clarke et al., 2002; Clarke and Rendell, 2006; review by Madsen and Murray, 2009) and also at the inland site of Breckland, East Anglia (Bateman and Godby, 2004).

During the climatic phase in NW Europe referred to as the Little Ice Age (LIA; AD1470–1900, Matthews and Briffa, 2005), the driving mechanism of storminess in the North Atlantic region was attributed by Lamb (1979) to an enhanced thermal gradient between

latitudes 55° and 65° N associated with a reduction in sea-surface temperatures in the North Atlantic, caused by the southward expansion of sea ice from the Arctic region. Clarke and Rendell (2009) compared archival records of sand movement in the North Atlantic coastal regions during the LIA and proxy records provided by the numerical dating results (OSL and radiocarbon). For phases of significant aeolian activity during the Holocene before the LIA, they made comparisons with the series of five quasi-periodic cooling events (8.2 ka, 5.9 ka, 4.2 ka, 2.8 ka and 1.4 ka) proposed by Bond et al. (1997), linking these with periods of increased storminess. They concluded that during the LIA numerous episodes of sand drift and dune formation on the western European coasts dated by OSL and radiocarbon could be linked to records of storminess, with sufficient indication of synchronicity to suggest that the climatic conditions leading to storminess were wide spread in northern Europe but, beyond the last millennium, comparison of the numerical dating evidence with the timing of the climatic cooling events yielded a correlation with only one of the events (8.2 ka) on a similar geographic scale. Since Clarke and Rendell's evaluation, further OSL ages for coastal dune formation within the N Atlantic coastal region have become available and these are also discussed below.

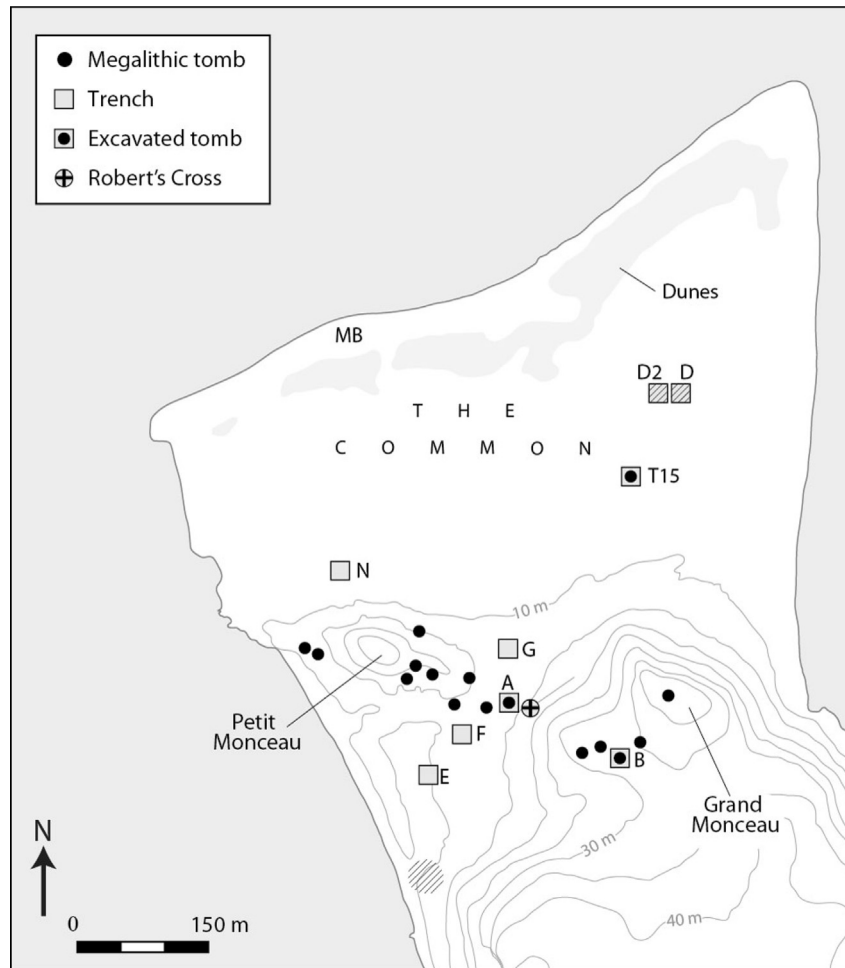


Fig. 2. Topographic plan of the middle and northern part of Herm showing the locations of Grand Monceau, Petit Monceau, the sixteen monuments, the trenches (A, B, D, D–G and N), the outcrop on Moussionnière Beach (MB) and excavated areas with evidence of settlement (cross hatched), as discussed in the main text.

2. The island setting and archaeology

In the northern part of Herm (Fig. 2) a rolling upland plateau formed on granodiorite descends to a northern lowland coastal plain, named The Common, which is covered by thick wind-blown sand deposits and dunes fronting the foreshore. In the central part of the saddle formed between the two hills of Petit Monceau (elev. 29 m) and Grand Monceau (elev. 43 m) lies the area of Robert's Cross in which the first trench, Trench A, was inserted on the north side of Tomb 12 (according to the numbering scheme adopted by Kendrick, 1928). The locations of eight of the excavation trenches (A, B, D, D2, E, F, G and N) and a barrier dune on the north shore (MB) investigated during four seasons (2008–2011) of excavation referred to in this paper are indicated in Fig. 2, and further details of the excavation and the palaeoenvironmental investigation can be found in Scarre and French (2013). The main objective of the Herm project was to investigate the buried land surfaces within areas of primary archaeological interest but, because of the ecological sensitivity in these areas, the trenches were necessarily limited in size. However, a comprehensive soil auger survey provided details of topographic features of the buried prehistoric landscape and two key features obscured by the blanketing sand were identified: a ridge projecting north from the foothills on which Tomb 15 (Fig. 2, T15) was located and, in the western part of the lowland plain, a shallow marine embayment containing 2 m of marine silts and fine sands sealed by 30 cm of peat development (formed between the

6th and 11th centuries AD on the basis of radiocarbon ages) and overlain by several metres of dune sand. The pollen and soil sequences obtained from analysis of the soil cores revealed an early Holocene landscape containing a wooded area around the edges of the marine embayment that was progressively degraded by human impact and climate and land that had been cultivated in areas north and south of Robert's Cross.

The detailed reconstruction of the landscape and soil development enabled the megalithic tombs to be placed within the palaeoenvironmental sequence and suggest that they were set within an agricultural landscape. One of the most striking features revealed in several of the trenches was the preserved evidence of cultivation. The finding of widely scattered Neolithic pot and flint fragments in the upper buried soil horizons, combined with indications of ard marks, in the form of shallow linear furrows created by a rudimentary plough, were interpreted as evidence of manuring to improve the fertility of the soils. From ca the 3rd or 2nd millennium BC onwards the coastal environment became increasingly marginal and there were prolonged intervals during the late prehistoric period and the late medieval period where cultivation appeared to have ceased due to the influx of sand. Evidence of settlement was found in two areas (Fig. 2), beneath a shoreline dune south of Petit Monceau and on The Common, east of a massive tabular outcrop that was investigated in Trenches D and D2. Although the deposits beneath the shoreline dune were heavily eroded, there was sufficient artefactual evidence to confirm early

Neolithic occupation, and the pottery and artefacts of the early 5th millennium BC recovered indicate that Herm has one of the few known earlier Neolithic settlements in the Channel Islands (Scarre and French, 2013), others being L'Erée and the Grand Hotel site on Guernsey (Sebire and Renouf, 2010; Cunliffe and de Jersey, 2000) and L'Ouzière and Mont Orgueil on Jersey (Marcigny et al., 2010).

3. The sampled contexts

3.1. Geomorphological investigation

The programme of soil sampling and analysis provided assessments of the nature and extent of the palaeosol horizons, guiding the selection of OSL samples. A full account of the geomorphological work, which followed the methodological approach described by Courty et al. (1989), is given elsewhere (French, 2011) and, drawing from that work, the main characteristics of the palaeosols and sands are described in the Supplementary Material (Section 1) and summarised in the following discussion of the sample locations.

The OSL samples were obtained from horizons at the nine locations indicated on the topographic plan (Fig. 2) and at depths indicated in the stratigraphic columns for each trench shown in Fig. 3 that are projected onto the two elevation transects (I and II), the positioning of which is marked on the plan (inset, Fig. 3). The trenches were located on Grand Monceau (B), in the Robert's Cross area (A, E, F, G) and on The Common (D, D2, and N), and the sampled location MB was located within the coastal dune fronting Mouissonnière Beach (MB; shown in Fig. 2 only). The sediments were sampled using opaque rigid plastic tubes (40 mm dia. in most cases) that were driven horizontally into cleaned sections to a depth of at least 20 cm, extracted and then promptly sealed to prevent exposure of the sediment to daylight and to retain the moisture content. At one location where the sediments were too compacted for the use of tubes (D2.2), blocks (at least $8 \times 3 \times 3$ cm) were cut from freshly exposed surfaces, shielded from sunlight, and stored in opaque material.

The basal dune sand and upper surface of buried soil were sampled above and below their contacts in Trenches A, D, D2, E, G, N and at the base of the MB dune. Trenches E and F provided access

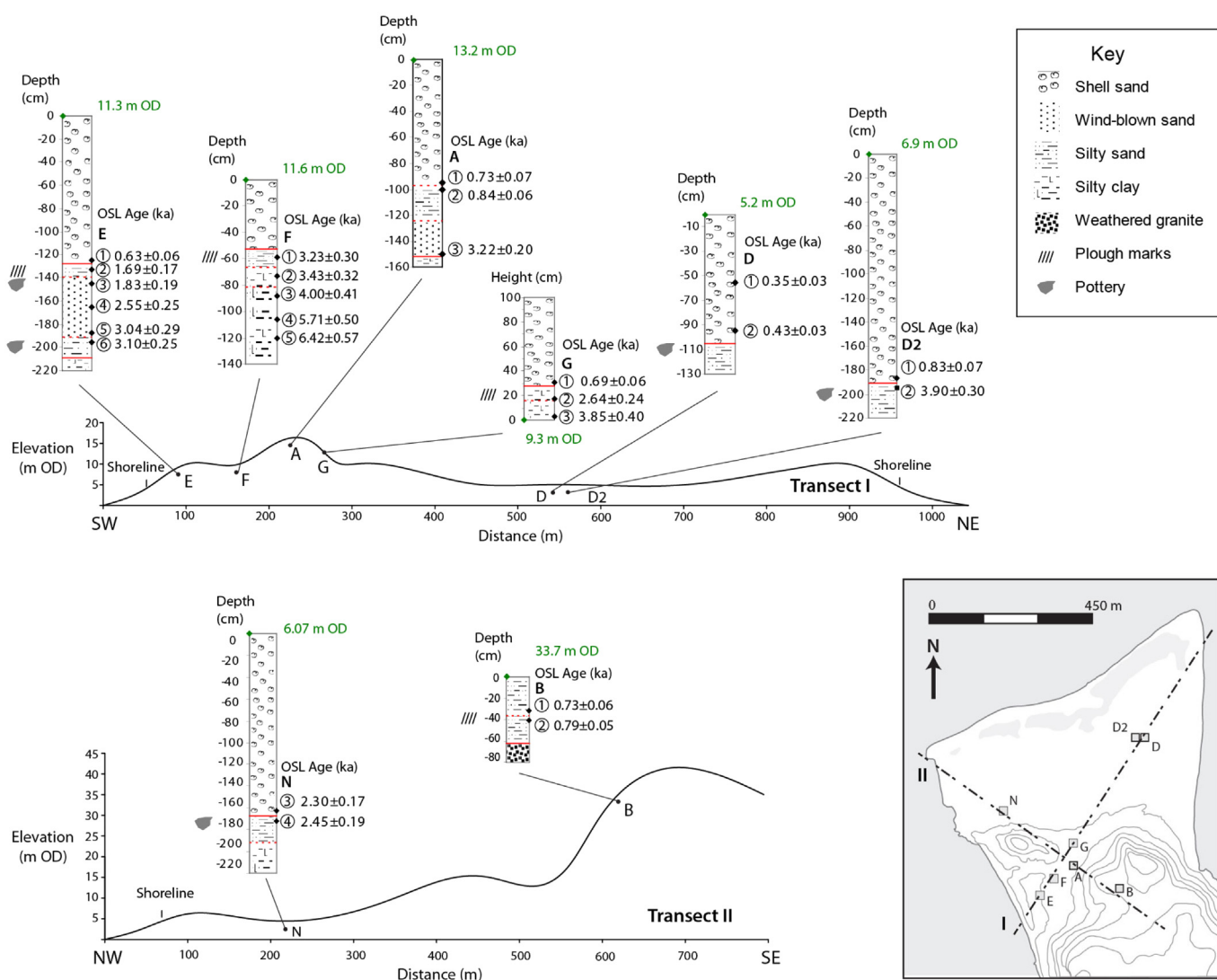


Fig. 3. Stratigraphy and OSL sample locations shown in two transects (I and II), the orientation of which are indicated on the map shown in the inset. The depths shown are below the ground surface at the sampled trench wall face (except Trench G, height above limit of excavation), the elevation of which is given at the top of each column relative to Ordnance Datum (OD). A solid red line in the columns represents the horizon boundary and a broken line indicates a gradual contact. The positions of the OSL sample tubes are indicated as filled circles and an excised block as a filled square (D2); the sample number within the trench is indicated to the right of the column, together with the OSL age and overall error (1σ). The location of sample MB.1 is shown in Fig. 2. (For interpretation of the references to colour in this figure legend, the reader is referred to the web version of this article.)

to well-preserved soil sequences and, as for Trenches B and G and MB, contained horizons with evidence of ploughing activity within the soil structure (indicated in Fig. 3, Trenches B, E, F and G). The positions of the OSL samples are discussed below as two groups, located south of The Common (in Trenches A, B, E and F) and on The Common (in Trenches D, D2 and N), including Mouisonnière Beach (MB).

3.2. South of The Common

On the northern side of the chambered tomb at Roberts Cross, Trench A was cut to investigate the structure of a suspected mound that covered the Northostats to the level of the capstones. Although no trace of an original mound was found in this trench, evidence for one was found in the 2011 excavations at the eastern end of tomb 12, and it is probable that it did once extend around the northern side of the chamber also. Its absence from Trench A must be the result of post-Neolithic erosion (supported by the OSL age obtained for the basal sand in this trench, as discussed below). Three OSL samples (Fig. 3, Transect I, A) were obtained from: A.1, basal sand dune deposits overlying an upper palaeosol; A.2, the upper palaeosol immediately below the contact with the dune deposits; A.3, a fine wind-blown sand overlying the basal palaeosol that was present closer to the tomb.

On the north-eastern side of Kendrick tomb 6 on Grand Monceau, Trench B had revealed a relatively shallow soil profile (ca. 65 cm), the structure of the upper part of which indicated a preserved land surface with visible evidence of individual plough marks and a ridge and furrow structure. The action of ploughing would have repeatedly exposed soil within several cm of the surface to daylight and hence potentially resulting in an optical bleaching (zeroing) process associated with the use of the land for cultivation. To investigate the temporal relationship between cultivation identified in this and the other trenches at lower elevation (G, E, F), two OSL samples were taken from the soils lying immediately above (B.1) and below (B.2) the buried land surface (Fig. 3, Transect II, B).

Within 50 m SW of Robert's Cross, Trench E provided sequences that extended from the Neolithic to the Roman periods, as indicated by the recovery of diagnostic pottery from basal and upper buried soil horizons. Lying below 125 cm of dune sand (Fig. 3, Transect I, E), the soil sequence contained at least two superimposed soils (for description, see [Supplementary Material](#), Section 1), separated by a stabilised windblown sand horizon. Six OSL sample cores (E.1–6) were positioned to sample four stages of land surface development: a) E.1, the formation of the overlying dune sand, b) the deposition of the upper palaeosol (E.2), c) the stabilisation and duration of the wind-blown sand (E.3, E.4 and E.5), and d) the later phase of development of the lower palaeosol (E.6). Both upper and lower palaeosols contained structural features attributed to ard-like plough marks. In Trench F, cut to examine the socket of a standing stone, three main soil horizons (Fig. 3, Transect I, F), the upper, middle and lower palaeosols were broadly similar in composition ([Supplementary Material](#), Section 1) to those in Trench E, differing in the proportions of wind-blown components. The structure of the upper palaeosol indicated disturbance caused by truncation and/or occasional ploughing and ard-marks were also visible in Trench F, especially in its southern section. The OSL sample cores were positioned to sample the later phases of deposition of the upper (F.1), middle (F.2) and lower (F.3) palaeosols and the earlier phases of development of the lower soil (F.4 and F.5).

The creation of a modern sand quarry pit north of Roberts Cross had enabled access to a preserved prehistoric land surface buried under dune deposits rising to a height of ca. 3 m. In Trench G two superimposed palaeosols extended to a depth of ~40 cm below the

contact with the dune sand and, within the trench area evidence of ard marks had been found in the dune sand/soil contact surface of the upper soil. Three OSL samples were located (Fig. 3, Transect I, G) immediately above (G.1) and below (G.2) the interface of the dune sand and upper palaeosol and at the base of the lower palaeosol (G.3).

3.3. The Common and Mouisonnière Beach

The timing of the burial of the prehistoric land surface by sand dune formation was examined in three trenches located on The Common (D, D2 and N) and at Mouisonnière Beach (MB). Trenches D and D2 had been cut to investigate a geophysical signature ([Scarre and French, 2013](#)) associated with a depression between massive granodiorite boulders that formed a bedrock outcrop 90 m north of Kendrick tomb 15. In Trench D (Fig. 3, Transect I, D), underlying about 1 m of shelly dune sand, excavation revealed a thin horizon of stabilized organic sand overlying a buried soil formed on the granodiorite bedrock. In the adjacent trench (Fig. 3, Transect I, D2) a greater depth (1.8 m) of dune sand covered a buried soil with characteristics similar to the upper palaeosol in Trench E, but much disturbed and likely to be the lower half of an *in situ* palaeosol. Fragments of prehistoric pottery and flint debitage had been recovered from the upper layers of the buried prehistoric soil in both D and D2, including, in the latter, a concentration of Neolithic pottery fragments which were possibly derived from a single vessel. The OSL samples were taken from the basal dune sand (D.2) in Trench D and, to gauge the rate of sand aggradation, at half the depth of the sand overlying the granodiorite outcrop (D.1). In Trench D2, a block of the palaeosol that included the buried land surface was cut and extracted (D2.2), together with a core of the overlying dune sand (D2.1). In Trench N, located on the northern slope at the base of Petit Monceau (Fig. 2), a truncated 15 cm-thick palaeosol was identified lying at a depth of ca 1.7 m below dune sand (Fig. 3, Transect II, N); a few prehistoric potsherds and struck flints were recovered from its upper part. The OSL samples were obtained immediately below and above the contact between the basal dune sand (N.4) and the upper part of the palaeosol (N.3). Finally, midway along Mouisonnière Beach and adjacent to a granodiorite outcrop, a 25 cm-thick palaeosol, lying 1.25 m above the upper beach level and developed on a weathered granodiorite substrate, was overlain by about 3.5 m of dune sand. OSL samples were taken from the basal dune sand deposits lying immediately above a buried soil (MB.1) judged to be of early Holocene age on the basis of geomorphological analysis ([Scarre and French, 2013](#)).

4. Experimental measurements

A summary of the experimental work is given in the following sections and further technical details are provided in the [Supplementary Material](#).

4.1. OSL characteristics

OSL dating procedures were applied to aliquots of quartz coarse grains (200–355 µm diameter) extracted from the sampled volumes of sediment. The equivalent dose, D_e , was determined using a single aliquot regenerative procedure (SAR), similar to that described by [Murray and Wintle \(2000, 2003\)](#) but with some minor differences in the measurement of sensitivity changes and thermal transfer ([Supplementary Material](#), Section 4, and [Table SM.1](#)). This procedure was extended by the use of an OSL scanner ([Bailiff and Mikhailik, 2003](#)) to determine the number of bright grains contributing to the detected luminescence in each aliquot and the use of relatively large grains increased the likelihood of obtaining

OSL intensities of sufficient strength with aliquots of samples extracted from the younger horizons. The quantity of grains deposited onto measurement discs was adjusted to minimise the number of bright grains in each aliquot, achieved by progressive adjustment of sample quantity and testing with the scanner. Using this approach about 70% of the aliquots yielding paleodose determinations contained a dominant single bright grain in the case of the dune sand and palaeosol samples, and a higher proportion (~80%) was obtained with aliquots of wind-blown sand samples (a breakdown of bright grain numbers is given in Table SM2, Supplementary Material). However, a high proportion (about 2/3rds) of the dune sand aliquots were discarded because of inadequate OSL signal strength ($<3 \times$ background signal intensity) and although the quantity of grains on each disc had been increased, this was constrained to a spread of ca 6–8 mm (employing a mask when spraying the discs with Si oil) to avoid a predominance of grains located near the periphery of the disc where there is a reduction in the dose rate from the beta source.

The OSL decay curves contained a dominant fast component (Supplementary Material, Section 3, Fig. SM1) and application of the early background (EBG) subtraction procedure confirmed the absence of significant changes in the value of D_e arising from the presence of the medium or slow decay components (Ballarini et al., 2007). The acceptance criteria (Wintle and Murray, 2006; Jacobs et al., 2006) for the recycling ratio, set at $\pm 10\%$ of unity, was met by a high proportion of the samples and the ratio averaged over all samples was 0.99 ± 0.04 (listed for each sample in Table SM2, Supplementary Material). The effect of preheat temperature on the evaluation of D_e was examined as part of the dose recovery experiment. A preheat plateau was obtained with most of the samples for preheat temperatures between 200 and 240 °C, and the overdispersion of the population of mean values obtained for the ratio D_e/D_a (where D_a is the applied dose) ranged between 5% and 15% (listed for each sample in Table SM2 and examples shown in Fig. SM2, Supplementary Material). A few samples exhibited higher levels of scatter in D_e , as reflected in the relative standard deviation (RSD) values, particularly in the case of three of the younger dune sand samples (A.2, 0.22; D.1, 0.26 and D.2, 0.19) and to a similar level with an older palaeosol sample (G.2, 0.19). A preheat temperature of 220 °C was applied when obtaining the D_e values used to construct the dose response curve and additional measurements were performed using a lower temperature preheat (200 °C) temperature to check for consistency in the determination of D_e for those samples where the RSD of the results of the dose recovery measurements had been in the higher range using a 220 °C preheat temperature.

4.2. Equivalent dose analysis

The equivalent dose, D_e , was evaluated following the SAR procedure by interpolation of the linear curve fitted to the dose response data. The distributions of the D_e values obtained were analysed using the central dose model (CDM; originally referred to as CAM, Central Age Model; Galbraith and Roberts, 2012; Galbraith et al., 1999; Roberts et al., 2000; Galbraith, 2005). The overdispersion calculated using the CDM is a statistical parameter of primary interest in analysing the distribution of the values of equivalent dose, D_e , and it provides a measure of the extent of variation in D_e in excess of that expected on the basis of instrumental errors. The causes of overdispersion are usually discussed in terms of 'extrinsic' and 'intrinsic' effects. Factors associated with the extrinsic effects include spatial heterogeneity in the beta dose rate and incomplete resetting of grains by sunlight at deposition. The intrinsic effects include those associated with the characteristics of the quartz (or selected mineral) and the overdispersion in the

values of D_e determined under the known applied dose conditions of the dose recovery experiment (Wintle and Murray, 2006) was used as a measure of the intrinsic uncertainty, σ_i for the Herm samples. The latter was combined in quadrature with the instrumental error associated with D_e (burial dose) to obtain the error estimate in the value of D_e analysed using the CDM. Although for dose recovery experiments the overdispersion is expected to be zero, it is evident in the recent literature that a considerable variation in the overdispersion estimates for quartz aliquots and single grains has been observed (e.g., Duller, 2012) and the values of σ_i for the Herm samples, expressed as percentages, fell within the range 4%–15% (Table 1, col. 7).

The weighted mean value of the paleodose (D_e) for each sample, together with the number of determinations (n) and the overdispersion calculated using the CDM (σ_b) are shown in Table 1 (with the exception of sample N.3 where D_e distribution was analysed using the finite mixture model, as discussed below); the values of overdispersion range from 0.06 to 0.31. In recent work on the mathematical modelling of D_e values for multi-grain mixtures of sediments, Arnold and Roberts (2009) compiled a list of published overdispersion values for quartz single grains and 'small-sized multi-grain' aliquots (<100 grains, estimated to contain between 4 and 16 bright grains inferred from empirical data in Duller et al., 2000) that were thought to comprise grains that had been fully bleached at deposition and not affected by post-depositional mixing. The mean values of the overdispersion for single aliquot and single-grain results, calculated using the CDM, were $14 \pm 7\%$ (s.d.; $n = 36$; range, 0–33%) and $20 \pm 7\%$ (s.d.; $n = 63$; range, 0–32%) respectively. The mean values of the overdispersion for the Herm samples are $18 \pm 7\%$ (s.d., $n = 25$; range, 6–31%) for single aliquots and $19 \pm 9\%$ (s.d., $n = 22$; range, 0–33%) when calculated using the results for aliquots containing a dominant single bright grain. The distribution of the latter is similar to that for the single grain data collected by Arnold and Roberts (2009; plotted as histograms in Fig. SM3, Supplementary Material). Although the published data in Arnold and Roberts' tabulation are drawn from a range of different types of site and depositional contexts, they show that a generally wide spread in overdispersion values is observed in sediments judged to be well bleached at deposition and that ostensibly, on the basis of overdispersion alone, the values for the Herm samples appear to be consistent with this pattern. It is worth noting that most of the published OSL dating work with coastal dune deposits has been performed with single aliquots (Madsen and Murray, 2009), and in these cases the values of overdispersion obtained will have been reduced by inter-grain averaging (Cunningham et al., 2011). Blumer et al. (2012), for example, examined late Holocene horizons within a perched dune field on the shores of Lake Michigan and obtained overdispersion values with small aliquots, each containing several thousand grains, ranging between 15 and 30% for D_e distributions described as log normal and unimodal.

However, as highlighted in earlier work by Bateman et al. (2003, 2007) and Bush and Feathers (2003) and examined by others (Boulter et al., 2006; Ahr et al., 2013; Stockmann et al., 2013), D_e distributions should be examined for statistically significant departures from a log-normal distribution of D_e values associated with the effects of post-depositional mixing caused by pedoturbation, bioturbation and other mixing mechanisms. Positive skewness may result, for example, from the presence of grains that were incompletely reset before burial and negative skewness may arise where grains from horizons of younger depositional age have become incorporated in the sampled horizon. The distributions of the Herm D_e values were analysed for skewness by calculating the weighted skewness score (Arnold and Roberts, 2009), c , for the results obtained with aliquots containing a single dominant bright grain since they allow the effects of intergrain differences to be

Table 1
OSL ages and related data.

Lab# 359-	Sample	Type	Dose rate			Equivalent dose				OSL age $\pm \sigma_B$ (ka)
			$\dot{D}_{\beta+ig} \pm \text{s.e.}$ (mGy a ⁻¹)	$\dot{D}_{\gamma+cos} \pm \text{s.e.}$ (mGy a ⁻¹)	$\dot{D}_{tot} \pm \text{s.e.}$ (mGy a ⁻¹)	Overdispersion $\sigma_i\%$	Overdispersion $\sigma_b\%$	n	$D_e \pm \text{s.e.}$ (Gy)	
7	A.1	DS	1.25 \pm 0.04	0.68 \pm 0.02	1.93 \pm 0.04	12	25	21	1.40 \pm 0.10	0.73 \pm 0.07
8	A.2	PS	1.21 \pm 0.04	0.70 \pm 0.02	1.91 \pm 0.04	10	11	13	1.59 \pm 0.08	0.84 \pm 0.06
6	A.3	WBS	0.76 \pm 0.02	0.66 \pm 0.02	1.42 \pm 0.03	7	15	25	4.58 \pm 0.17	3.22 \pm 0.20
9	B.1	PS	1.33 \pm 0.04	0.73 \pm 0.02	2.06 \pm 0.06	5	18	24	1.49 \pm 0.06	0.73 \pm 0.06
10	B.2	PS	1.22 \pm 0.04	0.79 \pm 0.02	2.01 \pm 0.06	5	16	17	1.59 \pm 0.08	0.79 \pm 0.05
12	D.1	DS	1.08 \pm 0.04	0.61 \pm 0.02	1.69 \pm 0.06	15	6	17	0.59 \pm 0.03	0.35 \pm 0.03
11a	D.2	DS	1.18 \pm 0.04	0.67 \pm 0.02	1.85 \pm 0.04	15	14	23	0.80 \pm 0.03	0.43 \pm 0.03
17.2	D2.1	DS	0.96 \pm 0.03	0.68 \pm 0.02	1.64 \pm 0.04	10	25	31	1.35 \pm 0.08	0.83 \pm 0.07
17.1	D2.2	PS	1.26 \pm 0.04	0.74 \pm 0.04	2.00 \pm 0.05	7	6	16	7.81 \pm 0.20	3.90 \pm 0.30
14.1	E.1	DS	1.20 \pm 0.04	0.74 \pm 0.02	1.94 \pm 0.04	11	13	9	1.22 \pm 0.07	0.63 \pm 0.06
14.2	E.2	PS	1.14 \pm 0.03	0.72 \pm 0.05	1.85 \pm 0.04	11	28	24	3.13 \pm 0.20	1.69 \pm 0.17
14.3	E.3	WBS	1.08 \pm 0.03	0.73 \pm 0.02	1.81 \pm 0.04	8	28	20	3.31 \pm 0.23	1.83 \pm 0.19
14.4	E.4	WBS	0.97 \pm 0.03	0.73 \pm 0.02	1.70 \pm 0.04	8	20	14	4.34 \pm 0.25	2.55 \pm 0.25
14.5	E.5	WBS	1.03 \pm 0.03	0.88 \pm 0.03	1.92 \pm 0.04	7	27	27	5.82 \pm 0.30	3.04 \pm 0.29
14.6	E.6	PS	1.18 \pm 0.04	0.87 \pm 0.03	2.05 \pm 0.04	10	8	26	6.36 \pm 0.20	3.10 \pm 0.25
15.1	F.1	PS	0.95 \pm 0.03	0.67(5) \pm 0.02	1.63 \pm 0.04	11	13	18	5.26 \pm 0.24	3.23 \pm 0.30
15.2	F.2	PS	1.17 \pm 0.04	0.77 \pm 0.02	1.94 \pm 0.04	7	16	18	6.64 \pm 0.31	3.43 \pm 0.32
15.3	F.3	PS	1.11 \pm 0.03	0.88 \pm 0.03	2.00 \pm 0.04	5	24	16	7.98 \pm 0.51	4.00 \pm 0.41
15.4	F.4	PS	1.13 \pm 0.03	1.09 \pm 0.03	2.22 \pm 0.05	10	17	31	12.70 \pm 0.62	5.71 \pm 0.50
15.5	F.5	PS	1.18 \pm 0.03	1.02 \pm 0.03	2.20 \pm 0.05	9	23	28	14.15 \pm 0.55	6.42 \pm 0.57
16.3	G.1	DS	0.89 \pm 0.03	0.72 \pm 0.02	1.61 \pm 0.03	12	24	25	1.10 \pm 0.06	0.69 \pm 0.06
16.2	G.2	PS	0.93 \pm 0.03	0.79 \pm 0.03	1.72 \pm 0.04	10	9	15	4.55 \pm 0.19	2.64 \pm 0.24
16.1	G.3	PS	1.32 \pm 0.04	0.69 \pm 0.02	2.01 \pm 0.04	9	23	17	7.14 \pm 0.45	3.85 \pm 0.40
18.2	N.3	DS	1.06 \pm 0.03	0.85 \pm 0.03	1.91 \pm 0.04	4	25	22	4.40 \pm 0.15	2.30 \pm 0.17
18.1	N.4	PS	1.22 \pm 0.04	0.85 \pm 0.03	2.07 \pm 0.04	8	13	25	5.07 \pm 0.16	2.45 \pm 0.19
22.1	MB.1	DS	1.01 \pm 0.03	0.87 \pm 0.03	1.89 \pm 0.04	6	31	42	1.09 \pm 0.06	0.58 \pm 0.05
(1)	(2)	(3)	(4)	(5)	(6)	(7)	(8)	(9)	(10)	(11)

1. Sediment type: DS, dune sand; PS, palaeosol; WBS, wind-blown sand.

2. Dose rate assessment. The values of the point absorber beta dose rate within the tested material, obtained using β -TLD, were reduced (by 16% for 200–355 μ m grains) to account for the effects of attenuation due to the finite size of the quartz grains using our calculations that are similar to those published by Brennan (2003). An allowance of 0.035 mGy a⁻¹ was made for the internal grain dose rate (alpha and beta) arising from radionuclides within the quartz. The gamma dose rate at each location was modelled using geometry factors derived from radiation transport simulations and taking into account the time-dependent development of overburden. Infinite medium dose rates were calculated using average measured radionuclide concentrations in the sediment sample(s) and conversion factors given by Adamiec and Aitken (1998) and those obtained from our own calculations. Corrections for moisture content were applied to both beta and gamma dose rates using factors (ratio of absorption coefficients for water and ceramic) of 1.25 and 1.14 for the beta and gamma dose-rates respectively, as calculated by Zimmerman (1971). The cosmic dose rate was calculated (Prescott and Hutton, 1988, 1994) for specified overburden in the dose rate model. The dose rates shown have been rounded to 2 decimal places.

3. Equivalent dose. With the exception of sample N.3, the weighted average values of D_e (col. 9) were calculated using the central dose model. The value of D_e shown for sample N.3 was calculated using the finite mixtures model, as discussed in the main text. The overdispersion σ_i was estimated by applying the central dose model to the dose recovery data; for each aliquot σ_i was combined in quadrature with the within-grain standard error to obtain variance in the burial dose D_e . The overdispersion σ_b was estimated by applying the central dose model to the n values of the burial dose D_e included in the analysis.

4. The reference year for age calculation is AD 2010.

better resolved. None of the values of c calculated (Table SM2, Supplementary Material) exceeded the critical skewness score for single grain samples ($2\sigma_c$; Arnold and Roberts, 2009; Bailey and Arnold, 2006). However, for D_e distributions with values of c corresponding to a high proportion of the critical value, combined with a value of overdispersion greater than the average (i.e., significantly above the average of 20%), there is the potential for the CDM to yield an under- or over- estimate of the burial dose. Depending on the polarity of the skewness and in these cases, it may be appropriate to analyse the distribution for D_e components using the finite mixture model (FMM; Roberts et al., 2000; Galbraith, 2005).

Of the three samples that exhibited relatively higher values of positive skewness and overdispersion, D2.1 ($c/2\sigma_c = 86\%$; $\sigma_b = 25\%$), F.5 ($c/2\sigma_c = 66\%$; $\sigma_b = 23\%$) and N.4 ($c/2\sigma_c = 54\%$; $\sigma_b = 13\%$), the distribution of D_e values for the dune sand sample D2.1 (radial plot shown in Fig. SM4a, Supplementary Material) has the strongest indication of the presence of grains either incompletely reset at deposition and/or originally associated with an older horizon. The application of the FMM identified two D_e components k1 ($D_e = 1.31 \pm 0.06$ Gy, 80%) and k2 ($D_e = 2.79 \pm 0.32$ Gy, 20%), where the percentages correspond to the proportion of aliquots in each component calculated by the model. The relatively

large uncertainty in the weighted mean value of D_e for k2 arises because of the small population of data values. The OSL ages, calculated using the values of D_e for k1 and k2 and using the same dose rate as shown in Table 1 for this location (1.64 ± 0.04 mGy a⁻¹), are 0.75 ± 0.06 ka and 1.60 ± 0.52 ka, respectively. The OSL age for k1 is only marginally earlier than that calculated with the value of D_e obtained by applying the CDM (Table 1, 0.80 ± 0.60 ka). Although the complex history of the dune sands and the highly dynamic nature of their deposition are likely to have given rise to the presence of grains of older depositional age in the basal deposits, the use of the simpler central dose model in this case appears sufficient.

The D_e distribution with the highest negative skewness score (but below the critical value for single grain samples, $2\sigma_c$) combined with a higher value of overdispersion is the dune sand sample N.3 ($c/2\sigma_c = 51\%$; $\sigma_b = 25\%$). Application of the FMM to the D_e distribution for N.3 resolved two components (radial plot shown in Fig. SM4b, Supplementary Material), k1 ($D_e = 4.40 \pm 0.15$ Gy, 40%) and k2 ($D_e = 6.64 \pm 0.20$ Gy, 60%). The lower value of D_e (k1), assumed to be associated with the most recently optically reset grains, yields an OSL age of 2.30 ± 0.17 ka. The presence of the higher dose component k2 identified by the FMM raises the question of the source(s) of the sand within the sampled context.

The OSL age calculated using the dose rate for the N.3 sampled volume ($1.91 \pm 0.04 \text{ mGy a}^{-1}$; Table 1) and the above value of D_e for k2 ($6.64 \pm 0.20 \text{ Gy}$) is $3.5 \pm 0.3 \text{ ka}$. Although the underlying horizon is a potential source of quartz grains of greater depositional age (i.e., if the sample tube had cut into the lower horizon), this outcome is unlikely since the OSL age of $2.45 \pm 0.19 \text{ ka}$ for the underlying palaeosol N.4 (Fig. 3, Transect II, N) is stratigraphically consistent with the OSL age for N.3 calculated using the D_e component k1 ($2.30 \pm 0.17 \text{ ka}$). On the other hand, the specific activities (Supplementary Material, Table SM3) of thorium and uranium in sample N.3 (Th, $15.3 \pm 2.8 \text{ Bq kg}^{-1}$; U, $17.4 \pm 1.6 \text{ Bq kg}^{-1}$) are closer to those of the palaeosols (ranges: Th, $13.4\text{--}33.4 \text{ Bq kg}^{-1}$; U, $10.2\text{--}31.2 \text{ Bq kg}^{-1}$) than the dune sands (excluding N.3, ranges: Th, $5.5\text{--}8.2 \text{ Bq kg}^{-1}$; U, $5.9\text{--}11.3 \text{ Bq kg}^{-1}$). Since the location of the sampled horizon is on the lower slope of Petit Monceau (Figs. 2 and 3) it is plausible, although speculative, that grains within a significantly older palaeosol unit upslope were reworked and combined with the basal dune sand at an early stage as part of a post-depositional mixing process (e.g., Bateman et al., 2007; Bueno et al., 2012) that occurred during the stabilisation of the dune.

Recent single grain work with very young deposits (<100 years; Costas et al., 2012a) has indicated that grains in dune sand horizons of at least several hundred years are likely to have been sufficiently reset. However, the degree of resetting will be dependent on local conditions that, under extreme storm conditions for example, could have varied significantly in terms of aerial transport. For the Herm samples, the values of overdispersion are relatively constrained and the application of the CDM, with the one exception of N.3, appears to be a sufficient statistical model to use for the determination of the dose accrued since burial. In the case of the dune sands, we have assumed that, following the onset of a period of aeolian activity, a series of cycles of deposition, deflation and reworking of sand (Fujioka and Chappell, 2010) occurred before a stabilized dune was formed and buried the sampled volume. In the case of the palaeosols the general absence of significant skewness in the D_e distributions suggests that the persistent input of aeolian sand, indicated by the micromorphological analysis, was a key component in the aggradation of the prehistoric soils, and that this has provided a means of obtaining OSL dates that relate temporally more closely to the process of the development of the soil horizons than would otherwise have been the case. However, in the absence of suitable radiocarbon samples from relevant horizons, it has not yet been possible to obtain an independent check of this temporal relationship.

4.3. Dose rate assessment

The average total dose rate to coarse quartz grains, \dot{D}_{tot} , was assessed taking into account lithogenic radionuclide sources located a) within the grains, emitting alpha and beta radiation and b) within the sediment medium external to the grains, emitting beta and gamma radiation, and c) cosmic radiation. External grain dose rates were measured directly using the experimental techniques of thermoluminescence dosimetry (β -TLD and γ -TLD; Supplementary Material, Section 5) and indirectly by measuring the radioactivity of sediment samples and calculating dose rates using published conversion factors (Adamiec and Aitken, 1998). In the β -TLD technique the active sample volume relevant to the measurement of the external dose rate is $\sim 0.25 \text{ cm}^3$, and for coarse grained sediments, such as the dune sands, replicate measurements with separately sampled volumes provided a means of testing for significant heterogeneity in radionuclide distribution, although not to the extent of providing a spatially resolved determination (Bailiff, 2011; Bailiff et al., 2013).

High resolution γ -ray spectrometry was used to measure the average specific activities (Bq kg^{-1}) of lithogenic radionuclides

contained in the sediment samples, the values of which (Supplementary Material, Table SM3) were used to calculate the contemporary dose rate within layers of infinite (β , γ) and semi-infinite thickness (γ). Different levels of average burial moisture content were adopted for three types of context, $15 \pm 3\%$ (dune sand), $20 \pm 4\%$ (interface, dune sand and palaeosol) and $25 \pm 5\%$ (palaeosol), based on the results of the measurement of contemporary moisture content of individual samples. The values of the average total burial dose rate, \dot{D}_{tot} , and its components, $\dot{D}_{\beta+\gamma}$ and $\dot{D}_{\gamma+\text{cos}}$, for each sample are listed in Table 1. $\dot{D}_{\beta+\gamma}$ represents the average beta dose rate, corrected for attenuation effects and average moisture content (Aitken, 1985), and includes a calculated contribution (0.035 mGy a^{-1}) to account for trace quantities of radionuclides within the grains. $\dot{D}_{\gamma+\text{cos}}$ represents the combined γ and cosmic burial dose rate, corrected for moisture content and each component of this combined dose rate, \dot{D}_{γ} and \dot{D}_{cos} , represents the time-averaged value of the burial dose rate for each location, as follows.

The gamma dose rate, \dot{D}_{γ} , within each sampled volume was calculated using a multiple-layer gamma dose rate model, developed for application in coastal contexts (Bailiff and Tooley, 2000), that uses geometry coefficients calculated by Løvborg and given in Aitken (1985; Appendix H). The spreadsheet-based model calculates the gamma dose rate at a selected depth within a sampled layer due to specified concentrations of the lithogenic radionuclides (U, Th and K) uniformly dispersed in each of five semi-infinite layers, two above and two below the designated sample layer, where the thickness of each layer can be varied from ca 1 cm upwards; the dose rate is also adjusted for moisture content specified in each layer. The model was applied to calculate the gamma dose rate at each sample position in a 'static' configuration, taking into account sediment strata of differing radionuclide content within $\sim 50 \text{ cm}$ of the sample position. The calculation provides an estimate of the gamma dose rate at the sample position in the current stratigraphy, but this does not necessarily represent the time-averaged dose rate since initial burial (apart from the adjustments made to account for moisture content). Following initial burial, the deposits lying beneath the sampled volume provide a half infinite medium for the gamma dose rate and thereafter the gamma dose rate increases during the development of overburden until its depth is sufficient to obtain an infinite medium dose rate ($\sim 50\%$ achieved at 5 cm and $\sim 95\%$ at 20 cm for a sediment with 25% moisture content). Where the time taken to achieve this condition is short relative to the burial period, the effect on the burial dose rate is usually negligible. However, if the palaeosol continued to aggrade and was subsequently eroded, followed at a later stage by sand dune development, the resulting gap in the sedimentary record also represents a missing part of the dose rate history, potentially affecting the time-averaged gamma dose rate for the burial period. As the depth of overburden increases there is a counteracting decrease in cosmic dose rate (Prescott and Hutton, 1988). At relatively shallow depths of overburden the variation in cosmic dose rate with depth is dominated by the attenuation of the 'soft' electron component that is removed by a depth of about 60 cm in sediment and the 'hard' muon component persists, reducing at a significantly lower rate with depth. At depths of ca 60, 100 and 200 cm below the ground surface, for example, the calculated cosmic dose rates are respectively 30%, 35% and 45% lower than the sub-surface dose rate ($\sim 0.29 \text{ mGy a}^{-1}$). Hence the cosmic dose rate was also calculated at each stage of overburden development model employing Prescott and Hutton's (1988) empirical depth—dose data. Using both types of calculation, the gamma and cosmic dose rates were calculated for the development of overburden from burial to the present surface. To illustrate the effect on the time averaged dose rate, three of the Herm locations

are examined, making use of the OSL age results and calculated rates of aggradation discussed in subsequent sections. The changes in gamma and cosmic dose rate components are expressed relative to the dose rate calculated using the static model.

Sample F.5 is representative of a sample located in the middle of a palaeosol sequence. On the basis of an aggradation rate of 13 cm per ka (Section 6.2), 95% of the infinite medium gamma dose rate (~ 26 cm) obtained by the addition of that layer is reached after a period of some 2 ka. The average gamma dose rate calculated for this period is $\sim 25\%$ lower than the infinite medium value (corresponding to a reduction of 0.06 mGy a^{-1} in the case of F.5), and this is compensated by a 36% increase in the average cosmic dose rate (corresponding to 0.07 mGy a^{-1}). The combined gamma and cosmic burial dose rate is consequently increased only marginally taking the overburden development into account and the difference in the dose rate obtained using the static and dynamic models is not significant. In sampled contexts of this type on Herm the dynamic model indicates that the static model calculation is adequate.

For an OSL sample located immediately below a land surface buried by dune sand, the history of overburden development is likely to be uncertain and this raises the issue of the effect of a higher cosmic dose-rate during the exposure of the land surface on the time-averaged total dose rate. Geomorphological analysis of the Herm palaeosol sequences indicated that the A horizons were truncated and consequently the process of aggradation is likely to have continued, followed by erosion to the preserved contact before the deposition of dune sand. During exposure of the prehistoric land surface, the cosmic dose rate would have been at its highest value (ca 0.29 mGy a^{-1}), and thereafter progressively diminished by dune formation, stabilisation and the addition of further sand deposits. In Trenches D2 and E, significant differences in the OSL age for the basal dune sand (D2.1, 0.83 ka; E.1, 0.63 ka) and the palaeosol located directly below the contact (D2.2, 3.9 ka; E.2, 1.69 ka) indicate gaps of about 3 ka and 1 ka respectively in the sedimentary record. If, in the case of the palaeosol in Trench D2, the prehistoric land surface had been exposed without further development of palaeosol or dune sand overburden, the model calculations indicate that the time-averaged gamma dose rate decreases by 20% (0.11 mGy a^{-1}) and that this is offset by a 60% increase in the cosmic dose rate (0.10 mGy a^{-1}). If, on the other hand, the aggradation of the palaeosol had continued, 90% of the infinite medium gamma dose rate would have been obtained within ~ 0.5 ka (corresponding to an overburden of 20 cm using a rate of 38 cm per ka; Section 6.2). As mentioned above and discussed further below, there was evidence in Trench A of a major post-Neolithic erosion event, followed by the deposition of wind-blown sand. If sand of similar composition had developed to a sufficient depth to provide an infinite medium until removal at some stage before stabilisation of dune sand during the medieval period, the calculated combined burial gamma and cosmic burial dose rate would be $\sim 5\%$ higher than the corresponding dose rate calculated using the static model, leading to a 2% increase in the total dose rate.

Although the context of the palaeosol sample E.2 was similar to that of D2.2, the lower depth of overburden (133 vs 194 cm for D2.2) and lower indicated time gap in the sediment record (~ 1 ka vs ~ 3 ka) give rise to a slightly different outcome. Applying the same approach as discussed for D2.2, exposure of the prehistoric land surface for a period of 1 ka gives rise to a calculated decrease of 20% (0.09 mGy a^{-1}) in the gamma dose rate and an increase of 40% in the cosmic dose rate (0.07 mGy a^{-1}) during the period of exposure, leading to a 2% reduction in the time-averaged combined gamma and cosmic dose rate for the (full) burial period. If the palaeosol continued to aggrade and sustained an average overburden of 20 cm for ~ 1 ka until eroded and replaced by dune sand, both calculated gamma and cosmic dose rates increase by 4%

(0.02 mGy a^{-1}) and 25% (0.04 mGy a^{-1}) respectively, relative to the static model, leading to a value of the time-averaged combined cosmic and gamma dose rate for the burial period that is 10% higher (by 0.06 mGy a^{-1}) than the static model, which corresponds to $\sim 3\%$ of the total dose rate.

Given the general geomorphological assessments of the upper palaeosol horizons, it is likely that the development of overburden had continued for locations currently lying immediately below the contact with dune sand, either in the form of palaeosol or dune sand. Although the duration of exposure of the prehistoric land surface remains uncertain, the modelled dose rate estimates indicate that the effect of prolonged exposure on the combined gamma and cosmic dose rate is relatively small ($<5\%$), and the adoption of a combined gamma and cosmic dose rate in the age calculation (Table 1) using a dynamic model based on overburden development of the type discussed above for D.2 and E.2 was considered a reasonable compromise. However in sedimentary contexts with very low radionuclide content where the cosmic dose rate forms a relatively high proportion of the total dose rate, the dependence of dose rate on overburden development is stronger and may require an iterative approach to estimating the time-averaged total dose rate when calculating the age (López and Thompson, 2012). Further details of the model calculations are given in Supplementary Material, Sec. 5.

4.4. OSL age calculation

The OSL ages were calculated by evaluating the quotient of the equivalent dose D_e and the average total dose rate, \dot{D}_{tot} (Table 1). The ages are given in the units of kilo-annum (ka), with calendrical date equivalents provided where discussion of archaeological aspects conventionally uses this timescale. They are given with type B ($\pm \sigma_B$) standard uncertainties (ISO, 1993) that were calculated at the 68% level of confidence (1σ) using a procedure based on an analysis of the propagation of errors, similar to that described by Aitken (1985). Type B standard uncertainty is based on an assessment of uncertainty associated with all the quantities employed in the calculation of the age, including those of type A standard uncertainty obtained by an analysis of repeated observations (i.e. random and systematic errors). The assessments are related to both the experimental results and the sample conditions that potentially may affect the values of parameters used in the calculation of the luminescence age.

5. Interpretation

As mentioned above, the key research questions to be addressed in this study were related to establishing the age of the prehistoric land surfaces, when they were buried and to obtain ages for key horizons in the prehistoric soil sequences. In interpreting the OSL ages obtained we first discuss the most recent phase of sand dune development and their contacts with the surviving prehistoric surfaces, and then to examine the timing of the development of the soils beneath them, including cultivation. Finally we examine the relationship between the signatures of significant aeolian activity within the Herm sedimentary deposits and those revealed at other sites within the wider N Atlantic region, and also more locally within the Normanno-Breton Gulf.

5.1. The burial of land surfaces by dune sand

The OSL ages (Table 1; Fig. 3) obtained for basal dune sands (shown in Fig. 3, transect I: A, A.1; D, D.2; D2, D2.1; E, E.1; G, G.1 and, in Fig. 2, location MB, MB.1) confirm that the onset of the accumulation of much of the substantial quantity of sand that now

blankets the north part of the island commenced during the medieval period, from the early 13th century (D2.1, 0.83 ± 0.07 ka; AD 1180 ± 70) and persisted until the late 16th century (D.1, 0.35 ± 0.03 ka; AD 1660 ± 30). South of the Common, the samples from Trenches A, E and D form a statistically coherent group (A.1, 0.73 ± 0.07 ka, E.1, 0.63 ± 0.06 ka and G.1, 0.69 ± 0.06 ka) with a pooled mean age of 0.69 ± 0.05 ka (AD 1320 ± 50) that, if assigned to the same phase of sand deposition, provides a measure of the reproducibility of the OSL ages for dune formation and stabilisation during this period.

In contrast, the OSL ages for the basal sands surrounding the granodiorite outcrop (D.2, 0.43 ± 0.03 ka (AD 1580 ± 30) vs D2.1, 0.83 ± 0.07 ka (AD 1180 ± 70)) that would have stood up to several metres above the prehistoric land surface are significantly different. The outcrop appears to have shielded the earlier medieval dune deposits (D2.2) from entrainment during substantial aeolian activity in the 17th century (D.1, 0.35 ± 0.03 ka; AD 1660 ± 30). The age for the basal sand at Mouisonnière Beach (MB.1, 0.58 ± 0.05 ka; AD 1430 ± 50), which places the dune consolidation in the early 15th century, indicates that the 14th century sand drift evident in the trenches south of The Common was part of an extended phase of significant modification of the dunes forming the coastal barrier.

Evidence of older dune formation was obtained in two trenches, in A (A.3, 3.22 ± 0.20 ka; 1210 ± 200 BC), adjacent to tomb 12 at Roberts Cross, and in N (N.3, 2.30 ± 0.17 ka; 290 ± 170 BC) on the lower north slope of Petit Monceau. This preservation may have resulted from shielding provided by the orthostats of tomb 12 (A) and by Petit Monceau (N) from west/south-westerly winds, characteristic of North Atlantic cyclones, during periods of significant sand drift. At these two locations the OSL ages for the basal dune sand underlying palaeosol horizons overlap, indicating a continuity in the transition from underlying incipient soil (A.2, 0.84 ± 0.06 ka; AD 1170 ± 60) to dune formation (A.1, 0.73 ± 0.07 ka; 1280 ± 70 AD). In Trench N the overlap of the basal fine wind-blown sand (N.3, 2.30 ± 0.17 ka; 290 ± 170 BC) and the underlying palaeosol (N.4, 2.45 ± 0.19 ka; 440 ± 190 BC) also indicates a relatively short delay before formation of the overlying dune.

Elsewhere, however, there is a gap in the sedimentary record between the uppermost palaeosol and the overlying dune sand and, moving closer to the coastal barrier, it progressively increases, as seen in Trenches E, G and D2 (Fig. 4). In Trench D2 the buried prehistoric land surface is some 3000 years older (D2.2, 3.90 ± 0.30 ka) than the overlying basal sand (D2.1, 0.83 ± 0.07 ka). As discussed further below, the lower palaeosol in Trench F, of similar age (F.3, upper layer, 4.00 ± 0.41 ka), was overlain by a very fine sandy loam with a strong wind-blown component that accumulated for several hundred years (F.2, 3.43 ± 0.32 ka). This suggests that the land surface surrounding the standing stone continued to be subjected to cycles of deposition of wind-blown sand and ephemeral dune development and deflation from the early 2nd millennium BC and it is likely that this instability continued on the northern part of The Common until the medieval period. Although there is evidence of truncation of the upper palaeosols in Trenches E and G associated with cultivation (Fig. 3, transect I; [Supplementary Material](#), Section 1), the absence of at least a millennium in the sedimentary record in both trenches again suggests a potentially unstable landscape during the early medieval period. In Trench A the composition of the upper palaeosol resembles a stabilised sand dune with incipient soil formation ([Supplementary Material](#), Section 1) and the late 12th century OSL date (A.2, 0.84 ± 0.06 ka; AD 1170 ± 60) obtained for the later phase of this horizon raises the possibility that the sedimentary record for the early medieval period was preserved within it. However the recovery of a fragment of diagnostic Roman pottery from the lower part of the horizon, together with other Roman material, indicates

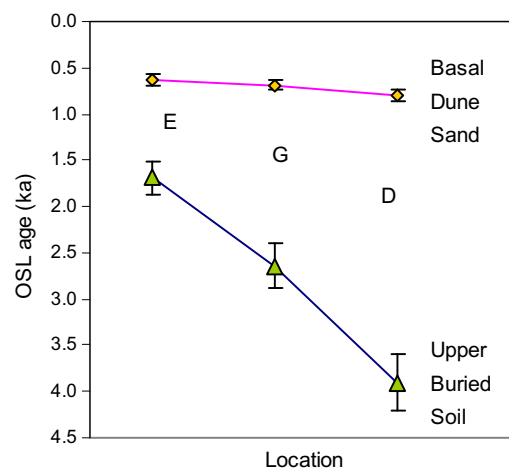


Fig. 4. Comparison of OSL dates for basal dune sand and the uppermost sample taken from the underlying prehistoric buried soil horizon, sampled in trenches E, G, D, the locations of which move progressively from trench E towards the northern dunes.

that to investigate this further OSL ages for intermediate levels within the horizon are required. In all the other trenches except N, where it may have survived, the early medieval horizon was obliterated by high aeolian activity at a much later stage, probably during the 13th or 14th centuries AD.

5.2. Prehistoric soil development

The OSL ages obtained for the samples from Trenches E and F provide two sequences that, combined, extend from the middle 5th millennium BC (F.5, 6.42 ± 0.57 ka; 4410 ± 570 BC) to the 4th century AD (E.2, 1.69 ± 0.17 ka; AD 320 ± 170 AD). The overlap of the OSL ages for the lower palaeosol in Trench E (E.6, 3.10 ± 0.25 ka; 1090 ± 250 BC) and the upper palaeosol in Trench F (F.1, 3.23 ± 0.30 ka; 1220 ± 300 BC) is consistent with the similarity of the geomorphological characteristics of the two palaeosols. Three OSL ages (E.3–E.5) for samples at the top, middle and base of the relatively deep horizon of windblown sand show that this phase of aeolian activity extends from the end of the 2nd millennium BC to the early 1st millennium AD, forming a key component of the surviving later prehistoric sedimentary record.

The trend in the rate of aggradation of the deposits is shown in Fig. 5 by plotting the OSL ages obtained for samples in Trenches E and F as a function of depth below the current ground surface. The OSL ages for Trench F indicate a significant change in the long term trend at the start of the 2nd millennium BC, the rate increasing from 13 ± 2 cm per ka (Fig. 5, I) to 38 ± 13 cm per ka (Fig. 5, II), marked by the onset of the formation of the middle palaeosol in Trench F which has a significant wind-blown component. The data for Trench E indicate that a similar long-term average rate of aggradation (41 ± 4 cm per ka) was maintained until the ca 4th century AD (E.2, 1.69 ± 0.17 ka; AD 320 ± 170). Although the trends in soil aggradation are based on the interpolation of a small number of data points spread over an extended timescale, the consistency of the OSL age for sample E.4, obtained from the middle of the wind-blown sand horizon, with the plotted trend line indicates that this horizon was not formed by a short-term influx of sand. During this period the process of clearance and ploughing would have made the early Holocene loess-rich soils susceptible to erosion and truncation and to sustain their viability for cultivation the soils were intensively manured from the late 4th millennium BC (Scarre and French, 2013). The aggradation of the palaeosols that developed during the Neolithic is attributed to the addition of fine wind-

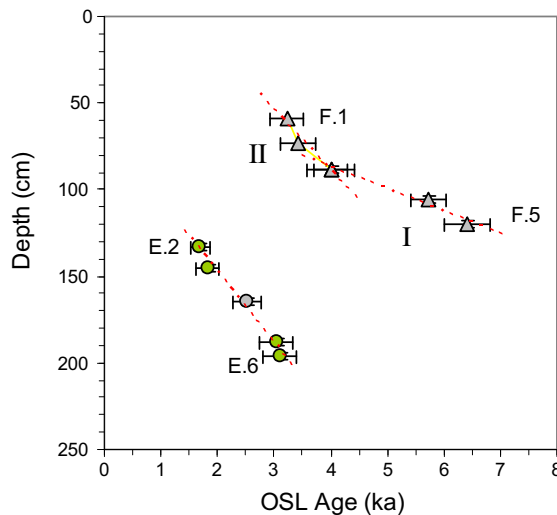


Fig. 5. OSL age–depth plots for samples from trenches E and F; the broken lines are indicative trend lines as discussed in the main text.

blown material and the relatively slow rate of accumulation that continued for two millennia from the middle of the 5th millennium BC to the early 2nd millennium BC is consistent with the micro-morphological assessment that the soils developed under relatively benign climatic conditions during the Neolithic.

The significant change in sand mobilization that occurred ca 4000 years ago would have required, in addition to winds of sufficient strength, a supply of sand. In one of the models applied to dune formation in Denmark (Christiansen et al., 1990), sand supply is influenced by relative sea level and tidal range, and during phases of falling sea level the increased exposure of the foreshore provides a greater area of sand available for aeolian transport. As observed by Seire and Renouf (2010), the lack of confirmed sea level index points (SLIPS) in the Normanno-Breton Gulf, the limited rise in mean sea level (msl, 2 m) during the last 7000 years predicted by the Lambeck model and the shallow waters surrounding Guernsey, give rise to significant uncertainty in estimating foreshore exposure based on change in msl. Given the large tidal range (10.3 m), a significant change (i.e., enlargement) of exposed foreshore ca 4000 years ago seems unlikely. However, while there appear to be differing views on the origin of the sands on northern Herm, erosion of the granodiorite shelf between Guernsey and Herm by periglacial weathering during the Late Pleistocene is likely to have provided a significant source of sand, as indicated by the presence of a very large sub-aqueous dune system within these shallow waters (Renouf, pers. comm.).

5.3. Cultivation

For the evidence for ploughing activity found in Trenches B, E, F and G and at MB, the OSL ages obtained indicate that the most recent cultivation was on Grand Monceau during the 13th century AD (Fig. 3, B.1, 0.73 ± 0.06 ka; AD 1280 ± 60 and B.2, 0.79 ± 0.05 ka; AD 1220 ± 50). By this time it is likely that viable arable soil was restricted to higher ground given the evidence of significant sand movement and dune formation on the lower lying land. Apart from the survival of the lower part of the palaeosol horizon in Trench A, any soil horizons that may have developed during the early medieval period have not survived, but the ploughing activity identified in the upper palaeosol on Trench E can be assigned to the late Roman period (E.2, 1.69 ± 0.17 ka; AD 320 ± 170). The OSL ages for the basal palaeosol in Trench E (E.6, 3.10 ± 0.25 ka; 1090 ± 250 BC) and the upper palaeosol in Trench F (F.1, 3.23 ± 0.30 ka; 1220 ± 300

BC) provide a consistent indication that cultivation was in progress during the late 2nd millennium BC. Evidence of ploughing activity was also detected in the upper surface of the palaeosol underlying the dune sand in Trench G and the OSL age obtained for this horizon (G.2, 2.64 ± 0.24 ka; 635 ± 240 BC) places its burial within a period of sustained influx of wind-blown sand during the 1st millennium BC when cultivation had been interrupted (Scarre and French, 2013). It is possible that the volume of soil sampled, which was at the edge of Trench G, had not been disturbed by ploughing (i.e., not exposed to daylight) and if this were the case, the OSL age obtained relates to the original (natural) deposition of the horizon.

5.4. Records of local and regional aeolian activity

The OSL ages for the dune sands discussed above (Section 5.1; A.1, D.1, D.2, D.2.1, E.1, G.1 and MB.1) identify significant aeolian activity extending across the late medieval period, in each of the 12th, 13th, 14th and 15th centuries AD, during which there are records of many storms in the North Atlantic region and their effect on coastal settlements. Lamb and Frydendahl (1991) identify ten of the most significant major storm events or sequences of storms in the history of the North Sea, of which five fall within the 12th–15th centuries AD (1200–1219, 1287, 1362, 1436 and 1570), and where, of all the historic storms, the 1570 storm was considered to have caused the most severe coastal flooding. While the precision of OSL is not sufficient to examine for specific correlations, the OSL dates (D.2.1, AD 1180 ± 70 ; the pooled mean of A.1, E.1 and G.1, AD 1320 ± 50 ; MB.1, AD 1430 ± 50 and D.2, AD 1580 ± 30) are consistent with the pattern of the most severe storms as chronicled by Lamb. Recent research (Renouf, pers. comm.) has identified a record of the effects of a severe storm in the Normanno-Breton Gulf, dated to ca 1332, where sand blow overwhelmed land on the Cotentin coast and this was linked, in a later source (Poingdestre, c1682, in Société Jersiaise 1889; Le Cornu, 1883), to the loss of land along the west coast of Jersey during the mid-14th century AD. The ca 1332 storm may have formed the initial event in a series of damaging storms that affected the Channel Islands during this period, the AD 1362 event chronicled by Lamb being the most intense.

The OSL age determinations for the prehistoric sand and palaeosol deposits (Section 5.2) place the onset of three phases of significant aeolian activity that modified the prehistoric landscape on Herm to ca 4 ka, 3 ka and 2.3 ka. To compare these phases of aeolian activity with those reported on a wider European scale, we turn to the series of studies mentioned earlier that have sought to examine the link between storminess and coastal dune formation. The OSL ages obtained for significant aeolian activity related to dunefields located on the coasts of: W Portugal (Clarke and Rendell, 2006; Clarke et al., 1999), SW France (Clarke et al., 2002), N Ireland (Wilson et al., 2004), NE England (Wilson et al., 2001), W Denmark (Clemmensen et al., 2009), Orkney and Shetland (Sommerville et al., 2001, 2003; 2007) and the Outer Hebrides (Gilbertson et al., 1999) are shown in Fig. 6. The OSL ages obtained by Bateman and Godby (2004) for the inland site of Breckland, East Anglia, are also included for comparison.

The study by Clemmensen et al. (2009) on dunefields on the west coast of Jutland also included radiocarbon determinations for thin intercalated horizons of peaty soil associated with phases of dune stabilisation. The addition of the Jutland and Herm ages to the dataset assessed by Clarke and Rendell (2006), provides a stronger indication of a potential correlation at a regional level of the OSL ages for two phases of significant aeolian activity, at ca 4 ka and 3 ka. The OSL ages obtained for the earliest phase of significant aeolian activity registered on Herm (ca 4 ka), Jutland (4.45 ± 0.18 ka) and Orkney (4.21 ± 0.14 ka) overlap (weighted

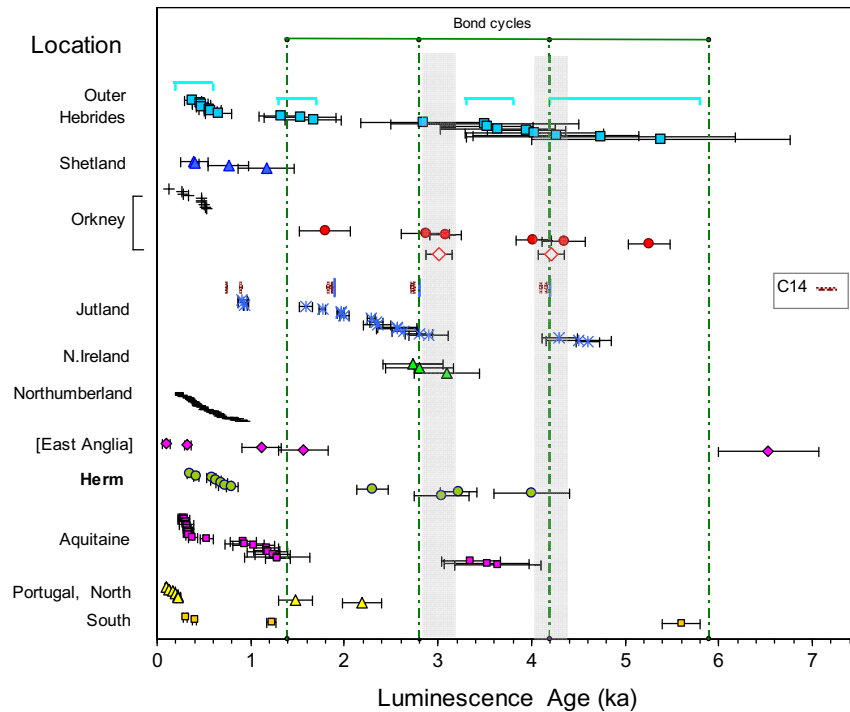


Fig. 6. Ages for aeolian activity on coastal dune sites in the North Atlantic region (basal sands). Comparison of Herm OSL dates with published results for nine studies discussed in the main text, from Portugal to Shetland. The sources of the OSL dates are: Portugal (South), [Costas et al., 2012b](#); Portugal (North), [Clarke and Rendell, 2006](#); Aquitaine, [Clarke et al., 2002](#); East Anglia, [Bateman and Godby, 2004](#) (shown within parentheses to distinguish its inland location); Northumberland, [Orford et al., 2000](#); Northern Ireland, [Wilson et al., 2004](#); Jutland, [Clemmensen et al., 2009](#); Orkney, [Sommerville et al., 2003, 2007](#); Shetland, [Sommerville et al., 2007](#); Outer Hebrides, [Gilbertson et al., 1999](#). Indicated above the sequence of Jutland OSL dates are calibrated radiocarbon ages (green bars) for underlying peaty soils interleaved in the sequence and red bars indicating the interpreted onset of dune formation. The two dates shown adjacent to the Orkney OSL dates (open diamonds) represent the weighted mean dates calculated by [Sommerville et al. \(2007\)](#). The bars shown adjacent to the sequence of the Outer Hebrides OSL dates represent the broad time periods of notable sand drift phases 4 (oldest) to 7 (most recent) assigned by [Gilbertson et al. \(1999\)](#). The vertical broken lines indicate the cooling phases proposed by [Bond et al. \(1997\)](#) and the vertical grey shaded bands represent the putative regional phases at 4.2 ka and 3 ka discussed in the main text. (For interpretation of the references to colour in this figure legend, the reader is referred to the web version of this article.)

mean age of 4.2 ± 0.2 ka using the age of E.3 for Herm) and similarly the OSL ages for the following phase on Herm (E.5, 3.04 ± 0.29 ka; A.3, 3.22 ± 0.20 ka), Ireland (2.84 ± 0.14 ka), Orkney (3.02 ± 0.14 ka) and Jutland (2.91 ± 0.17 ka; mean of ages for coastal dunes) also overlap (weighted mean age of 3.0 ± 0.2 ka). The OSL ages for the earliest phase of dune formation in the Aquitaine study, which are supported by radiocarbon ages for overlying and underlying organic layers ([Clarke et al., 2002, 1999](#)) form an exception to the above correlations, falling midway (3.35 ± 0.31 , 3.52 ± 0.46 and 3.65 ± 0.46 ka), between the putative regional correlations at ca 4 ka and 3 ka.

No OSL ages for dune formation on the north Brittany coast appear to have been published, but various studies have dated dune formation by obtaining radiocarbon determinations for associated organic samples ([Billeaud et al., 2009](#); [Meurisse-Fort, 2008](#); [Meurisse et al., 2005](#); [Bonnot-Courtois et al., 2002](#); [Haslett et al., 2000](#); [Regnaud et al., 1996](#)). Of the earlier dunes, ages for a palaeosol underlying the basal sands of perched dunes on the western coast of 4.2–4.6 ka cal BP ([Haslett et al., 2000](#)) and for a shell layer within dunes on the north coast ([Regnaud et al., 1996](#)) of 4.1–3.9 ka cal BP place the earliest dune formation to ca 4 ka ago which coincides with a regional phase as discussed above. Also [Guilcher and Hallégouët, \(1991\)](#) reported dune formation on the north coast (Marais de Dol, Gulf of St Malo) that was assigned a maximum age of 2.4 ka by association with a marine regression dated to the La Tène Iron Age period (similar to the third phase observed on Herm; N.3, 2.30 ± 0.17 ka; 290 ± 170 BC). A detailed study of the Holocene sedimentary record for Mont Saint Michel Bay by [Billeaud et al. \(2009\)](#) identified storm beds above erosional

surfaces and radiocarbon ages for shells sampled from the beds indicated enhanced storminess recurring on a millennial scale (5582–5706; 4783–4918; 4087–4325; 2910–3163; 1049–1232 cal BP), four of which (the exception being the second listed here) they argue match the sequence of cooling events identified by [Bond et al. \(1997\)](#). [Billeaud et al. \(2009\)](#) also observed that the sequence of climatic events in Spain ([Zazo et al., 2007](#)) and in Mont Saint Michel Bay are correlated. Since the events in NW France and Spain are expected to be accompanied by humid and arid conditions respectively, they suggest that an anticorrelation of conditions would have been obtained if the NAO was positive in NW Europe and negative in SW Europe. The similarity of the OSL age obtained by [Clarke and Rendell \(2006\)](#) for a phase of significant aeolian activity (2.19 ± 0.21 ka) on the west coast of Portugal with the OSL age for the third phase of aeolian activity on Herm (N.4, 2.30 ± 0.17 ka) appears to be consistent with the observation of [Billeaud et al. \(2009\)](#). The OSL ages for dune formation on the coasts of west Portugal and Aquitaine ([Clarke and Rendell, 2006](#)) were out of phase during the LIA, and Clarke and Rendell attributed this behaviour to differences in storm tracks controlled by the polarity of the North Atlantic Oscillation (NAO). However, in a recently published study of enhanced aeolian activity on the western coastline of Portugal (the Caparica coastal plain), [Costas et al. \(2012b\)](#) correlated ‘pulses’ of aeolian activity at 12.6, 5.6, 1.2, 0.44 and 0.3 ka, dated by OSL (Fig. 6), with four of the global cooling events of [Bond et al. \(1997\)](#), including the phases of enhanced aeolian activity in NW Europe during the LIA. In accounting for the absence of evidence for dune building associated with the third and fourth cooling events (i.e., dune forming conditions not suitable;

horizons not preserved or identified for sampling) they also refer to a Roman site 18 km south of their study area buried under transgressive dune building driven by northerly winds. While the sand depositional phases identified at Breckland, East Anglia (ca 6.5 ka, 1.6–1.1 ka, 0.5 ka, 0.40–0.34 ka and including a modern phase; Bateman and Godby, 2004) do not include the ca 4 ka and 3 ka phases of particular interest in the Herm study, Bateman and Godby suggested that, given the differences in the processes driving the formation of the dunes within inland and coastal regions, the existence of a correlation in the timing of several phases of aeolian activity on their inland site with those on coastal sites in the North Atlantic region dated using OSL indicated that the onset of aeolian activity had been activated by external climatic forcing.

Hence, not unexpectedly, the picture that is emerging regarding the relationship between climate change and dune formation, extending from the southern to northern coastlines of the North Atlantic, is complex and the chronometric dataset currently available for aeolian activity is thinly spread. However, identifying periods of significant aeolian activity during the Holocene is of particular importance in coastal regions because of the debilitating effect on cultivation caused by the rapid inundation of sand, and on small islands such events accentuate the vulnerability of settlements under these conditions.

6. Conclusion

In this study we have further developed the application of OSL dating of sands and palaeosol horizons, supported by geomorphological analysis, to identify critical stages in the development of the landscape on Herm. In particular, three phases of significant aeolian activity during the prehistoric period led to dune formation dated to ca 4 ka, 3 ka and 2.3 ka, where the first phase marked a significant increase in the long term trend of an aggradation of soils that persisted during the next two millennia. Palaeosols with structural evidence of disturbance consistent with ploughing were also tested and the OSL ages obtained for the sampled contexts place the activity in the late 2nd millennium BC and the 4th and 13th centuries AD. As discussed by Scarre and French (2013), cultivation in the northern part of the island appears to have been abandoned during a large part of the first millennium BC as a result of intensified aeolian activity.

The OSL ages for basal dune sands also revealed phases of aeolian activity during the medieval period, commencing in the C13th AD and persisting until the C17th AD, which probably account for most of the present blanket of sand covering the northern part of the island. These periods of enhanced aeolian activity can be correlated with documented high intensity storms in the North Atlantic within the period C13th–C15th AD, one of which in the Normanno-Breton Gulf can be connected to records of storm damage in Jersey. The phases of significant aeolian activity dated by OSL to ca 4 ka and 3 ka on Herm can be potentially linked with those detected in different regions of the North Atlantic coastal areas, a causal link with the quasiperiodic climatic cooling events being argued by Clemmensen et al. (2009) for three of their ages for aeolian activity on Jutland. In a recent proposal for the division of the Holocene Series/Epoch, Walker et al. (2012), who identify the 4.2 and 8.2 ka cooling events as the two significant stratigraphic markers of the Holocene defining the Middle–Late Holocene Boundary and the Early–Middle Holocene Boundary, respectively, suggest that these coincide with major catastrophic societal collapses in the archaeological record extending across northern Eurasia. Further investigation of these potential correlations of climatic change is of importance in terms of establishing a chronology for aeolian horizons that can be applied to the study of how past coastal communities responded to climate change. In terms of

the aeolian record, island settings such as those found on Herm may provide suitably preserved contexts for further study.

Acknowledgements

The fieldwork on Herm was supported by research award AH/F010575/1 from the Arts and Humanities Research Council. Special thanks are owed to the archaeology staff past and present of Guernsey Museum (Philip de Jersey, Heather Sebire, Tanya Walls and Jenny Cataroche) and to the Société Guernesaise for their assistance. Mr Adrian Heyworth (2008), Mr John Singer (2009–2011) and the States of Guernsey Environment Department kindly gave permission for us to work on Herm. Thanks are also offered to all the members of the Herm project team including students, volunteers, and specialists (Duncan Hale: geophysics; Dr Rob Scaife: palynology; Phil Howard: DTM and Dr John Renouf: geology); to Scott Grainger and Helen Drinkall for their contributions to laboratory work and to Dr Kate Sharpe for producing Figs. 1–3. We are grateful to Dr John Renouf and Dr Mike Church for comments on a draft version of the paper and we also thank two anonymous reviewers for their constructive comments.

Appendix A. Supplementary data

Supplementary data related to this article can be found at <http://dx.doi.org/10.1016/j.jas.2013.10.014>.

References

- Adamiec, G., Aitken, M.J., 1998. Dose rate conversion factors: update. *Ancient TL* 16, 37–50.
- Ahr, S., Nordt, L.C., Forman, S.L., 2013. Soil genesis, optical dating, and geoarchaeological evaluation of two upland Alfisol pedons within the tertiary gulf coastal plain. *Geoderma* 192, 211–226.
- Aitken, M.J., 1985. *Thermoluminescence Dating*. Academic Press, London.
- Arnold, L.J., Roberts, R.G., 2009. Stochastic modelling of multi-grain equivalent dose (D_e) distributions: implications for OSL dating of sediment mixtures. *Quat. Geochronol.* 4, 204–230.
- Bailiff, I.K., 2011. Spatially resolved measurement of beta dose rate using external dosimeters. In: Abstract. 13th International Conference on Luminescence and Electron Spin Resonance Dating, 10–14 July 2011, Toruń, Poland.
- Bailiff, I.K., Lewis, S.G., Drinkall, H.C., White, M.J., 2013. Luminescence dating of sediments from a Palaeolithic site associated with a solution feature on the North Downs of Kent, UK. *Quat. Geochronol.* 18, 135–148.
- Bailiff, I.K., Mikhailik, V., 2003. Spatially resolved measurement of optically stimulated luminescence and time-resolved luminescence. *Radiat. Measurements* 37, 151–159.
- Bailiff, I.K., Tooley, M.J., 2000. Luminescence dating of fine-grain Holocene sediments from a coastal setting. In: Shennan, I., Andrews, J. (Eds.), *Holocene Land-ocean Interaction and Environmental Change Around the North Sea*. Geological Society Special Publications, 166. Geological Society, London, pp. 55–67.
- Bailey, R.M., Arnold, L.J., 2006. Statistical modelling of single grain quartz D_e distributions and an assessment of procedures for estimating burial dose. *Quat. Sci. Rev.* 25, 2475–2502.
- Ballarini, M., Wallinga, J., Wintle, A.G., Bos, A.J.J., 2007. A modified SAR protocol for optical dating of individual grains from young quartz samples. *Radiat. Measurements* 42, 360–369.
- Bateman, M.D., Frederick, C.D., Jaiswal, M.K., Singhvi, A.K., 2003. Investigations into the potential effects of pedoturbation on luminescence dating. *Quat. Sci. Rev.* 22, 1169–1176.
- Bateman, M.D., Godby, S.P., 2004. Late-Holocene inland dune activity in the UK: a case study from Breckland, East Anglia. *Holocene* 14, 579–588.
- Bateman, M.D., Boulter, C.H., Carr, A.S., Frederick, C.D., Peter, D., Wilder, M., 2007. Detecting post-depositional sediment disturbance in sandy deposits using optical luminescence. *Quat. Geochronol.* 2, 57–64.
- Billeaud, I., Tessier, B., Lesueur, P., 2009. Impacts of late Holocene rapid climate changes as recorded in a macrotidal coastal setting (Mont-Saint-Michel Bay, France). *Geology* 37, 1031–1034.
- Blumer, B.E., Arbogast, A.F., Forman, S.L., 2012. The OSL chronology of eolian sand deposition in a perched dune field along the northwestern shore of Lake Michigan. *Quat. Res.* 77, 445–455.
- Bond, G., Showers, W., Cheseby, M., Lotti, R., Almasi, P., de Menocal, P., Priore, P., Cullen, H., Hajdas, I., Bonani, G., 1997. A pervasive millennial-scale cycle in North Atlantic Holocene and glacial climates. *Science* 278, 1257–1266.

- Bonnot-Courtois, C., Caline, B., L'Homer, A., Le Vot, M., 2002. La Baie du Mont-Saint-Michel et l'Estuaire de la Rance: environnements sédimentaires, aménagements et évolution récente. Pau, CNRS, EPHE & TotalFinaElf.
- Boulter, C.H., Bateman, M.D., Carr, A.S., Frederick, C.D., 2006. Assessment of archaeological site integrity of sandy substrates using luminescence dating. *Newsl. Soc. Archaeol. Sci.* 29 (2), 8–12.
- Brennan, B.J., 2003. Beta doses to spherical grains. *Radiat. Measurements* 37, 299–303.
- Bueno, L., Feathers, J., De Blasis, P., 2012. The formation Processes of an open-air site in Central Brazil: integrating lithic analysis, radiocarbon and luminescence dating. *J. Archaeol. Sci.* 40, 190–203.
- Bush, D.A., Feathers, J.K., 2003. Application of OSL single-aliquot and single-grain dating to quartz from anthropogenic soil profiles in the SE United States. *Quat. Sci. Rev.* 22, 1153–1159.
- Christiansen, C., Dalsgaard, K., Möller, J.T., Bowman, D., 1990. Coastal dunes in Denmark in relation to sea level. In: Bakker, Th. W., Jungerius, P.D., Klijn, J.A. (Eds.), *Dunes of the European Coasts*, Catena Supplement 18, pp. 61–70.
- Clarke, M.L., Rendell, H.M., Pye, K., Tastet, J.-P., Pontee, N.I., Masse, L., 1999. Evidence for the timing of dune development on the Aquitaine Coast, southwest France. *Z. Geomorphol. Suppl. Band* 116, 147–163.
- Clarke, M., Rendell, H., Tastet, J.-P., Clavé, B., Massé, L., 2002. Late-Holocene sand invasion and North Atlantic storminess along the Aquitaine Coast, southwest France. *Holocene* 12, 231–238.
- Clarke, M.L., Rendell, H.M., 2006. Effects of storminess, sand supply and the North Atlantic oscillation on sand invasion and coastal dune accretion in western Portugal. *Holocene* 16, 341–355.
- Clarke, M.L., Rendell, H.M., 2009. The impact of North Atlantic storminess on western European coasts: a review. *Quat. Int.* 195, 31–41.
- Clemmensen, L.B., Andreasen, F., Heinemeier, J., Murray, A., 2001. A Holocene coastal aeolian system, Vejers, Denmark: landscape evolution and sequence stratigraphy. *Terra Nova* 13, 129–134.
- Clemmensen, L.B., Murray, A., Heinemeier, J., de Jong, R., 2009. The evolution of Holocene coastal dune fields, Jutland, Denmark: a record of climate change over the past 5000 years. *Geomorphology* 105, 303–313.
- Costas, I., Reimann, T., Tsukamoto, S., Ludwig, J., Lindhorst, S., Frechen, M., Hass, H.C., Betzler, C., 2012a. Comparison of OSL ages from young dune sediments with a high-resolution independent age model. *Quat. Geochronol.* 10.
- Costas, S., Jerez, S., Trigo, R.M., Goble, R., Rebêlo, L., 2012b. Sand invasion along the Portuguese coast forced by westerly shifts during cold climate events. *Quat. Sci. Rev.* 42, 15–28.
- Courty, M.-A., Goldberg, P., Macphail, R.I., 1989. *Soils and Micromorphology in Archaeology*. Cambridge University Press, Cambridge.
- Cunliffe, B., de Jersey, P., 2000. Rescue excavations on Guernsey and Herm, 1998, 1999. *Trans. Soc. Guernesaise* 24, 867–944.
- Cunningham, A.C., Wallinga, J., Minderhoud, P.S.J., 2011. Expectations of scatter in equivalent dose distributions when using multi-grain aliquots for OSL dating. *Geochronometria* 38, 414–431.
- Duller, G.A.T., Bøtter-Jensen, L., Murray, A.S., 2000. Optical dating of single sand-sized grains of quartz: sources of variability. *Radiat. Measurements* 37, 543–550.
- Duller, G.A.T., 2012. Improving the accuracy and precision of equivalent doses determined using the optically stimulated luminescence signal from single grains of quartz. *Radiat. Measurements* 47, 770–777.
- French, C., 2011. The Holocene Soil and Landscape Development of the Northern Part of the Island of Herm (unpublished report).
- Fujioka, T., Chappell, J., 2010. History of Australian aridity: chronology in the evolution of arid landscapes. In: Bishop, P., Pillans, B. (Eds.), *Australian Landscapes*. Geological Society, London, Special Publications 346, pp. 121–139.
- Galbraith, R.F., 2005. *Statistics for Fission Track Analysis*. Chapman and Hall/CRC Press, Boca Raton, Florida.
- Galbraith, R.F., Roberts, R.G., Laslett, G.M., Yoshida, H., Olley, J.M., 1999. Optical dating of single and multiple grains of quartz from Jinmium rock shelter, Northern Australia: part 1, experimental details and statistical models. *Archaeometry* 41, 339–364.
- Galbraith, R.F., Roberts, R.G., 2012. Statistical aspects of equivalent dose and error calculation and display in OSL dating: an overview and some recommendations. *Quat. Geochronol.* 11, 1–27.
- Gilbertson, D.D., Schwenninger, J.-L., Kemp, R.A., Rhodes, E.J., 1999. Sand-drift and soil formation along an exposed North Atlantic coastline: 14,000 years of diverse geomorphological, climatic and human impacts. *J. Archaeol. Sci.* 26, 439–469.
- Guilcher, A., Hallégouët, B., 1991. Coastal dunes and their management. *J. Coast. Res.* 517–533.
- Haslett, S.K., Davies, P., Curr, R.H.F., 2000. Geomorphologic and palaeoenvironmental development of Holocene perched coastal dunes systems in Brittany, France. *Geogr. Ann.* 82A, 79–88.
- ISO, 1993. *International Vocabulary of Basic and General Terms in Metrology*, second ed. International Organisation for Standardization, Geneva, Switzerland.
- Jacobs, Z., Duller, G.A.T., Wintle, A.G., 2006. Interpretation of single grain D_e distributions and calculation of D_e . *Radiat. Measurements* 41, 264–277.
- Kendrick, T.D., 1928. *The Archaeology of the Channel Islands*. In: *The Bailiwick of Guernsey*, vol. I. Methuen and Co., London.
- Lamb, H.H., 1977. *Climate, Present Past and Future: Climatic History and the Future*, vol. 2. Methuen & Co, London.
- Lamb, H.H., 1979. Climatic variations and changes in the wind and ocean circulation: the Little Ice Age in the North-east Atlantic. *Quat. Res.* 11, 1–20.
- Lamb, H.H., Frydendahl, K., 1991. *Historic Storms of the North Sea, British Isles and Northwest Europe*. Cambridge University Press, Cambridge.
- Le Cornu, C.-P., 1883. Recueil de matières historiques, touchant les envahissements de la mer dans les parages de la baie de St-Ouen. *Bull. Ann. Soc. Jersiaise* 1, 385–396.
- López, G.I., Thompson, J.W., 2012. OSL and sediment accumulation rate models: understanding the history of sediment deposition. *Quat. Geochronol.* 10, 175–179.
- Madsen, A.T., Murray, A.S., 2009. Optically stimulated luminescence dating of young sediments: a review. *Geomorphology* 109, 3–16.
- Marcigny, C., Ghesquière, E., Juhel, L., Charraud, F., 2010. Entre Néolithique ancien et Néolithique moyen en Normandie et dans les îles anglo-normandes. *Parcours chronologique*. In: Billard, C., Legris, M. (Eds.), *Premiers Néolithiques de l'Ouest*. Cultures, réseaux, échanges des premières sociétés néolithiques à leur expansion. Presses Universitaires de Rennes, Rennes, pp. 117–162.
- Matthews, J.A., Briffa, K.R., 2005. The 'Little Ice Age': re-evaluation of an evolving concept. *Geogr. Ann. Ser. A Phys. Geogr.* 87, 17–36.
- Meurisse, M., van Vliet-Lanøe, B., Talon, B., Recourt, P., 2005. Complexes dunaires et tourbeux holocènes du littoral du Nord de la France. *C. R. Géosci.* 337, 675–684.
- Meurisse-Fort, M., 2008. *Enregistrement haute résolution des massifs dunaires: Manche, mer du Nord et Atlantique. Le rôle des tempêtes*. Éditions Publibook, Paris.
- Murray, A.S., Wintle, A.G., 2000. Luminescence dating of quartz using an improved single-aliquot regenerative-dose protocol. *Radiat. Measurements* 32, 57–73.
- Murray, A.S., Wintle, A.G., 2003. The single aliquot regenerative dose protocol: potential for improvements in reliability. *Radiat. Measurements* 37, 377–381.
- Orford, J.D., Wilson, P., Wintle, A.G., Knight, J., Braley, S., 2000. Holocene coastal dune initiation in Northumberland and Norfolk, eastern UK: climate and sea-level changes as possible forcing agents for dune initiation. In: Shennan, I., Andrews, J. (Eds.), *Holocene Land-ocean Interaction and Environmental Change Around the North Sea*. Geological Society, London, Special Publications 166, pp. 197–217.
- Prescott, J.R., Hutton, J.T., 1988. Cosmic ray and gamma ray dosimetry for TL and ESR. *Radiat. Measurements* 14, 223–227.
- Prescott, J.R., Hutton, J.T., 1994. Cosmic ray contribution to dose rates for luminescence and ESR dating: large depths and long-term time variations. *Radiat. Measurements* 23, 497–500.
- Regnaud, H., Jennings, S., Delaney, C., Lemasson, L., 1996. Holocene sea-level variations and geomorphological response: an example from northern Brittany (France). *Quat. Sci. Rev.* 15, 781–787.
- Roberts, R.G., Galbraith, R.F., Yoshida, H., Laslett, G.M., Olley, J.M., 2000. Distinguishing dose populations in sediment mixtures: a test of single-grain optical dating procedures using mixtures of laboratory-dosed quartz. *Radiat. Measurements* 32, 459–465.
- Scarre, C.J., French, C.A., 2013. The palaeogeography and Neolithic archaeology of Herm. *J. Field Archaeol.* 38, 1–15.
- Seibre, H., Renouf, J., 2010. Sea change: new evidence for Mesolithic and Early Neolithic presence in the Channel Islands with particular reference to Guernsey and the rising Holocene sea. *Oxf. J. Archaeol.* 29, 361–386.
- Société Jersiaise, 1889. *Caesarea or a Discourse of the Island of Jersey*. le Lieutenant-Bailli Jean Poingdestre, pp. 74–75.
- Sommerville, A.A., Sanderson, D.C.W., Hansom, J.D., Housley, R.A., 2001. Luminescence dating of aeolian activity sands from archaeological sites in Northern Britain: a preliminary study. *Quat. Sci. Rev.* 20, 913–919.
- Sommerville, A.A., Hansom, J.D., Sanderson, D.C.W., Housley, R.A., 2003. Optically stimulated luminescence dating of large storm events in Scotland. *Quat. Sci. Rev.* 22, 1085–1092.
- Sommerville, A.A., Hansom, J.D., Housley, R.A., Sanderson, D.C.W., 2007. Optically stimulated luminescence (OSL) dating of coastal aeolian sand accumulation in Sanday, Orkney Islands, Scotland. *Holocene* 17, 627–637.
- Stockmann, U., Minasny, B., Pietsch, T.J., McBratney, A.B., 2013. Quantifying processes of pedogenesis using optically stimulated luminescence. *Eur. J. Soil Sci.* 64, 145–160.
- Walker, M.J.C., Berkelhammer, M., Björck, S., Cwynar, L.C., Fisher, D.A., Long, A.J., Lowe, J.J., Newnham, R.M., Rasmussen, S.O., Weiss, H., 2012. Formal subdivision of the Holocene Series/Epoch: a discussion paper by a working group of INTIMATE (Integration of ice-core, marine and terrestrial records) and the Subcommission on Quaternary Stratigraphy (International Commission on Stratigraphy). *J. Quat. Sci.* 27, 649–659.
- Wilson, P., McCourt, J.M., Bateman, M.D., 2004. Mid-to late-Holocene coastal dune event stratigraphy for the north coast of Northern Ireland. *Holocene* 14, 406–416.
- Wilson, P., Orford, J.D., Knight, J., Braley, S.M., Wintle, A.G., 2001. Late-Holocene (post-4000 years BP) coastal dune development in Northumberland, northeast England. *Holocene* 11, 215–229.
- Wintle, A.G., Clarke, M.L., Musson, F.M., Orford, J.D., Devoy, R.J.N., 1998. Luminescence dating of recent dunes on Inch Spit, Dingle Bay, southwest Ireland. *Holocene* 8, 331–339.
- Wintle, A.G., Murray, A.S., 2006. A review of quartz optically stimulated luminescence characteristics and their relevance in single-aliquot regeneration dating protocols. *Radiat. Measurements* 41, 369–391.
- Zazo, C., Dabrio, C.J., Goy, J.L., Lario, J., Cabero, A., Silva, P.G., Bardaji, T., Mercier, N., Borja, F., Roquero, E., 2007. The coastal archives of the last 15 ka in the Atlantic-Mediterranean Spanish linkage area: sea level and climate changes. *Quat. Int.* 181, 72–87.
- Zimmerman, D.W., 1971. Thermoluminescent dating using fine grains from pottery. *Archaeometry* 13, 29–52.